Model-data comparison of Antarctic winter sea-ice extent and Southern Ocean sea-surface temperatures during Marine Isotope Stage 5e

Matthew Chadwick[1], Louise C Sime[2], Claire S Allen[2], and M- Vittoria Guarino[3]

[1]Cornwall Insight
[2]British Antarctic Survey
[3]International Centre for Theoretical Physics

December 22, 2022

Abstract

Marine Isotope Stage (MIS) 5e (130-116 ka) represents a 'process analogue' for future anthropogenic warming. Climate model simulations for MIS 5e have previously failed to produce Southern Ocean sea-surface temperatures (SST) and sea-ice extent reconstructed from marine sediment core proxy records. Here we compare state of the art HadGEM3 and HadCM3 simulations of Peak MIS 5e Southern Ocean summer SST and September sea-ice concentrations with the latest marine sediment core proxy data. The model outputs and proxy records show the least consistency in the regions located near the present-day Southern Ocean gyre boundaries, implying that model simulations are currently unable to fully realise changes in gyre extent and position during MIS 5e. Including Heinrich 11 meltwater forcing in Peak MIS 5e climate simulations improves the likeness to proxy data but it is clear that longer (3-4 ka) run times are required to fully test the consistency between models and data.

1   **Model-data comparison of Antarctic winter sea-ice extent and Southern**

2   **Ocean sea-surface temperatures during Marine Isotope Stage 5e**

3   M. Chadwick[1,2*]; L.C. Sime[1]; C.S. Allen[1] & M.-V. Guarino[1,3]

4   *[1.] British Antarctic Survey, Cambridge, UK*

5   *[2.] Ocean and Earth Science, University of Southampton, Southampton, UK*

6   *[3.] Earth System Physics Section, International Centre for Theoretical Physics, Trieste, Italy*

7   *Corresponding author:* m.chadwick@cornwall-insight.com, British Antarctic Survey, High Cross, Madingley Rd.,
8   CB3 0ET, Cambridge, UK

9   **Key points**

10 -   Different areas of the Southern Ocean show different consistency between model simulations
11   and proxy data.
12 -   Inclusion of Heinrich 11 meltwater forcing improves the match between model simulations
13   and proxy data.

14 **Abstract**

15 Marine Isotope Stage (MIS) 5e (130-116 ka) represents a 'process analogue' for future anthropogenic

16 warming. Climate model simulations for MIS 5e have previously failed to produce Southern Ocean

17 sea-surface temperatures (SST) and sea-ice extent reconstructed from marine sediment core proxy

18 records. Here we compare state of the art HadGEM3 and HadCM3 simulations of Peak MIS 5e

19 Southern Ocean summer SST and September sea-ice concentrations with the latest marine sediment

20 core proxy data. The model outputs and proxy records show the least consistency in the regions

21 located near the present-day Southern Ocean gyre boundaries, implying that model simulations are

22 currently unable to fully realise changes in gyre extent and position during MIS 5e. Including Heinrich

23 11 meltwater forcing in Peak MIS 5e climate simulations improves the likeness to proxy data but it is

24 clear that longer (3-4 ka) run times are required to fully test the consistency between models and

25 data.

26 **Plain Language Summary**

27 Investigating past warm periods can provide us with an analogue for how climate will respond to

28 future warming. In this study we compare the latest computer simulations of Southern Ocean sea-

29 surface temperatures and Antarctic winter sea-ice extent from 130,000 years ago with data from

30 marine sediment cores. The simulations and sediment core data show the least match in the areas

31 near the boundaries of the present day Southern Ocean gyres (large, circulating ocean currents),

32 implying that changes in the position and size of the gyres are not fully recreated in the computer

33 simulations. The inclusion of ice sheet meltwater into the North Atlantic improves the comparison

34 between the simulations and sediment core data but it is clear that longer simulation run times are

35 required to fully test their consistency.

36 **Keywords**

37 Last interglacial; Southern Ocean; sea ice; sea-surface temperatures; model-data comparison

38 **1. Introduction**

39 In the present day, Antarctic winter sea ice covers an area of ~1.8 x 10^6 km^2 and forms a critical

40 component of the global climate system (Maksym 2019). Sea ice has a high albedo or 'reflectivity' (Hall

41 2004), and seasonal growth in sea ice influences the strength of Southern Ocean (SO) and global

42 overturning circulation through the formation of dense Antarctic shelf and bottom waters

43 (Abernathey et al. 2016, Rintoul 2018). Rising atmospheric greenhouse gas concentrations are driving

44 current global warming, with a predicted reduction of 24-34 % in the Antarctic winter sea-ice extent

45 (WSIE) by 2100 (Meredith et al. 2019). The short length of the observational record for Antarctic sea

46 ice, coupled with the complex climate dynamics involved in changes to modern WSIE (Hobbs et al.

47 2016, Purich et al. 2016) mean that model simulations have been unable to faithfully replicate recent

48 changes in Antarctic sea ice unless they use unrealistically reduced warming (Rosenblum & Eisenman

49 2017). Marine Isotope Stage (MIS) 5e proxy records offer valuable evidence of a 'warmer-than-

50 present' climate, and the opportunity to improve our understanding/prediction of the impacts of

51 future climate change.

52 During MIS 5e (130-116 ka) both mean annual global atmospheric temperatures and mean annual SO

53 sea-surface temperatures (SSTs) peaked at ~2 °C warmer than preindustrial (PI) (Capron et al. 2017,

54 Fischer et al. 2018). Global sea levels were also 1.2-5.3 m higher than the present day (Dyer et al.

55 2021). Unlike future anthropogenic warming, MIS 5e warming is forced by orbital changes, alongside

56 a variety of internal ocean-ice-atmosphere feedbacks, rather than being driven by increasing

57 atmospheric greenhouse gas concentrations. However, MIS 5e represents an important 'process

58 analogue' for understanding the climatic mechanisms and feedbacks active under warmer-than-

59 present climates (Stone et al. 2016).

60 Model simulations of the Peak MIS 5e climate at 127 ka are a part of the Coupled Model

61 Intercomparison Project (CMIP6) and Paleoclimate Modelling Intercomparison Project (PMIP4) (Otto-

62 Bliesner et al. 2017). Analysis of the short (50-100 years) orbitally forced CMIP6-PMIP4 ensembles

63 indicate that these simulations exhibit SO summer $SSTs_{model}$ (SSSTs) which were ~0.5 °C cooler during

64 Peak MIS 5e than the PI and that there was an average reduction of ~5-8 % in WSIE at 127 ka relative

65 to the PI (Otto-Bliesner et al. 2021). These simulation results are a poor match for published Peak MIS

66 5e proxy records from SO marine sediment cores, which indicate a $SSST_{proxy}$ warming of 0-5 ^{o}C relative

67 to the PI (Capron et al. 2017, Otto-Bliesner et al. 2021). The SO model-data discrepancy is hypothesised

68 to be due to the absence of the Heinrich 11 (H11) meltwater event in CMIP6-PMIP4 Tier 1 simulations

69 (Otto-Bliesner et al. 2021). Though we also note that model-data comparisons of MIS 5e Antarctic

70 WSIE have been limited by the location of most published marine sediment core records: they are

71 located north of the modern WSIE, and likely also north of the 127 ka WSIE (Holloway et al. 2017,

72 Chadwick et al. 2020).

73 The published syntheses of proxy records from SO marine sediment cores in Capron et al. (2017) and

74 Chadwick et al. (2020) indicate Peak MIS 5e $SSSTs_{proxy}$ were between 0 and 5 ^{o}C warmer than the

75 present and PI, with this warming anomaly decreasing towards the South Pole. The most southerly

76 marine cores in these syntheses have $SSST_{proxy}$ anomalies for Peak MIS 5e of <1.5 ^{o}C (40 ^{o}W – 40 ^{o}E),

77 but there are no MIS 5e marine records located south of the modern Antarctic Polar Front (APF) for

78 most of the SO (80 ^{o}E – 40 ^{o}W).

79 Whilst most proxy records of Antarctic sea ice are located too far north to precisely constrain the Peak

80 MIS 5e $WSIE_{proxy}$, a recent reconstruction suggests that the winter sea-ice (WSI) edge was located 1-2°

81 south of its modern position in the Pacific sector and >5° south of its modern position in the Atlantic

82 sector (Chadwick et al. 2022a).

83 This study presents a new model-data comparison for the Southern Ocean during MIS 5e. Peak MIS

84 5e Antarctic September sea-ice concentrations (SIC_{model}) and SO $SSSTs_{model}$ from the latest UK fully-

85 coupled HadGEM3-GC3.1 (hereafter HadGEM3) numerical simulations, both with and without the H11

86 meltwater event (Guarino et al. 2022, *in review*), and from the H11 meltwater-hosed HadCM3

87 numerical simulations in Holloway et al. (2018) are compared with the latest diatom transfer function

88 estimates of September SIC_{proxy} and $SSSTs_{proxy}$ from nine marine sediment cores (Chadwick et al. 2021,

89 Chadwick et al. 2022a) to answer the following:

90   - Can we now tell if different areas of the Southern Ocean show more or less consistency
91   between model simulations and proxy data during MIS 5e?

92   - Is H11 meltwater forcing necessary for the models to match the proxy records?

93   - Are our current state of the art models capable of simulating the proxy data?

2. Materials and methods

2.1. Numerical simulations

94 HadGEM3 is a global coupled atmosphere-land-ocean-ice model which combines the Unified Model
95 Atmosphere model (Walters et al. 2017), the JULES land surface model (Walters et al. 2017), the NEMO
96 ocean model (Madec et al. 2019) and the CICE sea-ice model (Ridley et al. 2018b). The PI control run
97 is presented in Menary et al. (2018) and uses a constant 1850 climate forcing (see Menary et al. (2018)
98 for further details).

99 The standard Peak MIS 5e simulation (hereafter referred to as LIG_HG) is published in Guarino et al.
100 (2020) and the H11 simulation is published in Guarino et al. (2022, *in review*). They were run using the
101 protocol described in Otto-Bliesner et al. (2017) for Tier 1 and Tier 2 PMIP4 simulations. The Peak MIS
102 5e climate was simulated by forcing the HadGEM3 model with constant last interglacial orbital and
103 greenhouse gas boundary conditions (see Guarino et al. (2022, *in review*) for further details). In the
104 H11 run, the H11 meltwater event is simulated by adding a constant freshwater flux equal to 0.2 Sv,
105 evenly across the North Atlantic between 50 and 70 °N (Otto-Bliesner et al. 2017). The H11 simulation
106 was run for 250 years with the climatological averages from the final 100 years (150-250 years)
107 presented here (hereafter referred to as H11(250)_HG).

108 HadCM3 is a faster running, but older and lower resolution, UK model than HadGEM3. The HadCM3
109 simulations are published in Holloway et al. (2018), with 0.25 Sv freshwater forcing to the North
110 Atlantic applied for 1600 years. We use the climatological averages for years 150-250 of the model
111 run (hereafter referred to as H11(250)_HC), to match the length of the run performed for HadGEM3,
112 and the last 100 years (1500-1600 years)(hereafter referred to as H11(1600)_HC), to examine how
113 $SSSTs_{model}$ and $SICs_{model}$ evolved after a longer period of H11 type forcing.

114 MIS 5e $SSSTs_{model}$ (average January to March) are presented as anomalies relative to the PI control
115 runs whereas September $SICs_{model}$ are presented as absolute values.

2.2. Marine sediment cores

116 Modern Analog Technique diatom transfer function estimates of September $SICs_{proxy}$ and $SSSTs_{proxy}$ for
117 Peak MIS 5e, reconstructed from nine marine sediment cores and published in Chadwick et al. (2022a),
118 are compared to model output. The transfer function methodology is detailed in Chadwick et al.
119 (2022a) and the data for all the cores is available from Chadwick et al. (2021). Reconstructed
120 September $SICs_{proxy}$ have a Root Mean Square Error of Prediction (RMSEP) of 0.09 and $SSSTs_{proxy}$ have
121 a RMSEP of 1.1 °C. For PI $SSSTs_{proxy}$ at each core site the average January-March SST_{proxy} from 1870-
122 1900 was calculated from the HadISST1 dataset (Rayner et al. 2003). The average $SSST_{proxy}$ and

126 September SIC$_{proxy}$ in the 130-128 ka interval is considered to represent Peak MIS 5e conditions. This

127 time interval is chosen as it is within the chronological uncertainty (±2 ka) of both the peak δ^{18}O in the

128 EPICA Dome C ice core record at ~128 ka (Sime et al. 2009) and the termination of the H11 meltwater

129 event at 130 ka (Marino et al. 2015).

3. Results

3.1. SSST$_{model}$ anomalies

132 In both the LIG_HG and H11(250)_HG simulations the pattern of SSST$_{model}$ anomalies for Peak MIS 5e

133 relative to the PI is very similar (Figure 1a & b). Both runs show a cooling (0-1 °C) in the Atlantic sector

134 (70 °W – 20 °E) and a warming (0-1.5 °C) in the Indian sector (20 – 150 °E) during Peak MIS 5e relative

135 to the PI, with both trends more pronounced in the H11(250)_HG run (Figure 1b). In the Pacific sector

136 (150 °E – 70 °W), both the LIG_HG and H11(250)_HG simulations show a warming (0-1 °C) in the

137 eastern region (120 – 70 °W) and a cooling (0-0.5 °C) in the western region, south of the modern WSIE

138 (150 °E – 150 °W) but have diverging trends in the central area (150 – 120 °W) where the LIG_HG run

139 has a warming of up to 1 °C and the H11(250)_HG run has a mixture of warming and cooling, all by

140 less than 0.5 °C (Figure 1a & b).

141 The H11(250)_HC and H11(1600)_HC simulations both have greater warming trends than either of the

142 HadGEM3 runs, with only a few localised areas of cooling in the H11(250)_HC run and none in

143 H11(1600)_HC run (Figure 1c & d). In the H11(250)_HC run, the area north of the modern WSIE had

144 largely warmed by 0.5-1.5 °C, whereas the region within the modern WSIE was generally less than 0.5

145 °C warmer than PI (Figure 1c). In the H11(1600)_HC run the SSST$_{model}$ anomalies have increased

146 throughout the SO relative to the H11(250)_HC run, with the region within the modern WSIE mainly

147 0.5-1.5 °C warmer than PI and the area to the north of the modern WSIE largely showing 1-3 °C

148 warming (Figure 1d). All simulations show the greatest Peak MIS 5e warming in the 90-170 °E region,

149 north of 60 °S (Figure 1).

3.2. SSST$_{proxy}$ anomalies

151 With the exception of core TPC290, the sediment cores all indicate warmer conditions during Peak

152 MIS 5e than the PI (Table 1 & Figure 1). The Pacific sector cores have SSST$_{proxy}$ anomalies of less than

153 1.5 °C, with the more southerly cores showing a warming of less than 1 °C (Table 1). The nearby cores

154 TPC288 and TPC287 in the Atlantic sector have similar SSST$_{proxy}$ anomalies to each other, whereas, in

155 the Indian sector, the proximally located cores MD03-2603 and U1361A have very different SSST$_{proxy}$

156 anomalies to each other, with the SSST$_{proxy}$ anomaly for core MD03-2603 more than 3 °C warmer than

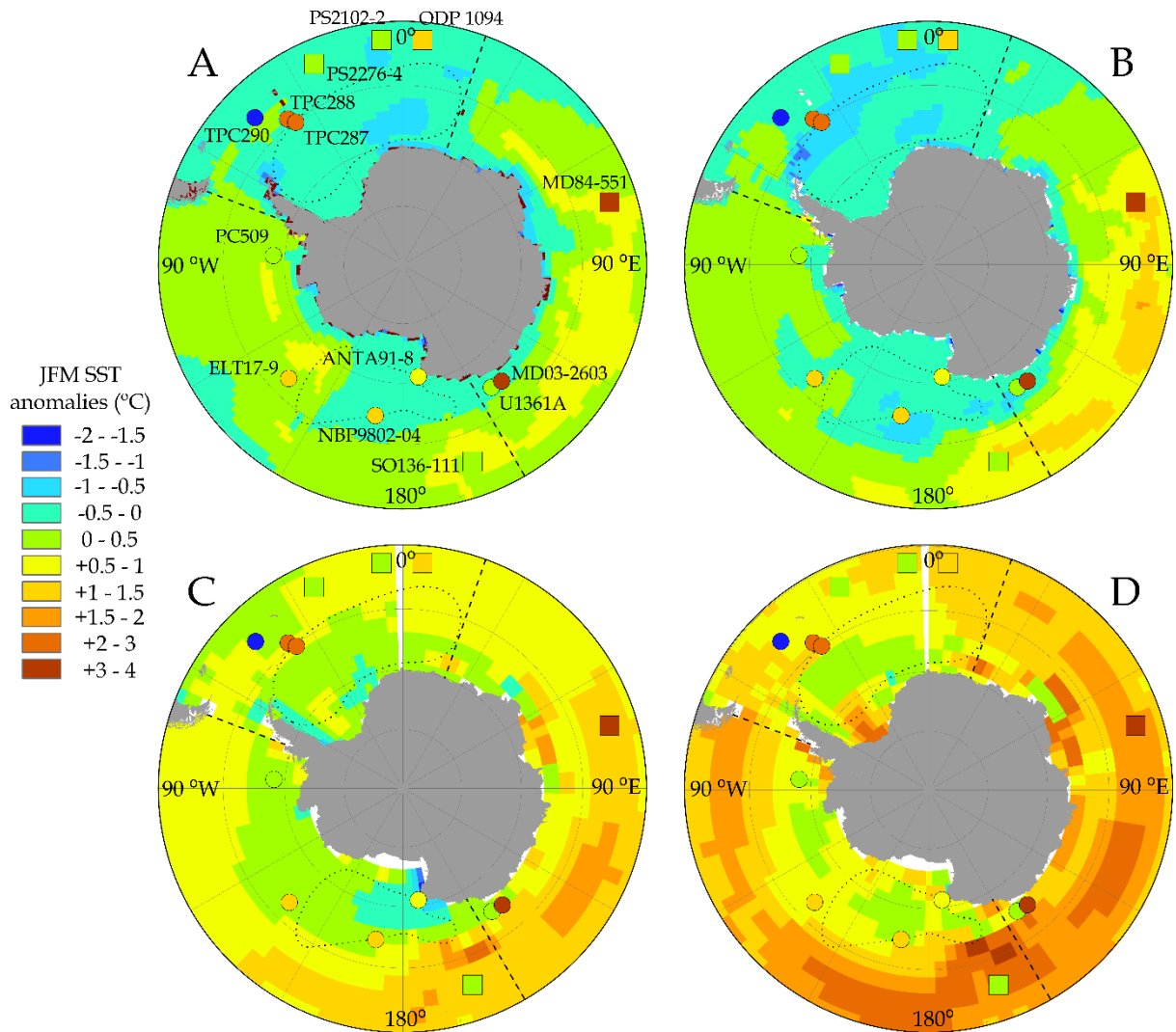157 the anomaly in core U1361A (Table 1 & Figure 1).

Figure 1: Maps of summer (JFM) SST_{model} anomalies for Peak MIS 5e relative to the PI. **A** - LIG_HG. **B** - H11(250)_HG. **C** - H11(250)_HC. **D** - H11(1600)_HC. Coloured circles on all maps represent the JFM SST_{proxy} anomalies from Chadwick et al. (2022a) and coloured squares represent the summer SST_{proxy} anomalies from Capron et al. (2017). The dashed black lines mark the boundaries between the three SO sectors and the dotted black lines mark the modern extents of the Weddell Sea and Ross Sea gyres (positions of the Weddell Sea gyre is from Vernet et al. (2019) and the Ross Sea gyre is from Dotto et al. (2018)).

158   Within the ±1.1 °C uncertainty on the diatom transfer function $SSST_{proxy}$ values and the standard

159   deviation of the model output, the Peak MIS 5e – PI $SSST_{proxy}$ anomalies in all Pacific sector cores match

160   the H11(250)_HC and H11(1600)_HC runs (Table 1, Figure 1c & d). Proxy data for cores PC509 and

161   ANTA91-8 also match the HadGEM3 model outputs (Table 1) and the proxy data in core ELT17-9

162   matches the LIG_HG run (Table 1). The transfer function Peak MIS 5e $SSST_{proxy}$ anomaly in core U1361A

163   also matches, within uncertainty, the values from all four model runs (Table 1). The transfer function

164   $SSST_{proxy}$ anomalies in cores TPC288 and MD03-2603 only match the model output for H11(1600)_HC

165   and in core TPC287 there is not a match with any of the model outputs considered here (Table 1).

166 Cores TPC288, TPC287 and MD03-2603 have SSST$_{proxy}$ anomalies >2 °C warmer than all the models and

167 core TPC290 >1.5 °C cooler than all the models (Table 1).

	TPC290	TPC288	TPC287	ELT17-9	NBP9802-04	MD03-2603	U1361A	PC509	ANTA91-8	SO average (mean ± st. dev.)
Latitude (°S), Longitude (°E)	55.55, -45.02	59.14, -37.96	60.31, -36.65	63.08, -135.12	64.20, -170.08	64.28, 139.38	64.41, 143.89	68.31, -86.03	70.78, 172.83	-
SSST$_{proxy}$ anomaly (°C)	-1.70 ± 1.10	+2.65 ± 1.10	+2.75 ± 1.10	+1.24 ± 1.10	+1.43 ± 1.10	+3.13 ± 1.10	+0.04 ± 1.10	+0.24 ± 1.10	+1.00 ± 1.10	+1.56 ± 1.19
LIG_HG SSST$_{model}$ anomaly (°C)	-0.03 ± 0.67	-0.19 ± 0.90	-0.31 ± 1.02	+0.19 ± 0.91	-0.32 ± 1.06	-0.19 ± 1.05	-0.20 ± 1.18	+0.25 ± 1.01	-0.10 ± 0.29	-0.10 ± 0.04
H11(250)_HG SSST$_{model}$ anomaly (°C)	-0.16 ± 0.60	-0.50 ± 0.90	-0.78 ± 0.92	-0.03 ± 1.11	-0.55 ± 1.00	-0.50 ± 1.07	-0.66 ± 1.17	-0.02 ± 0.83	-0.13 ± 0.26	-0.37 ± 0.07
H11(250)_HC SSST$_{model}$ anomaly (°C)	+0.45 ± 0.72	+0.67 ± 0.82	+0.62 ± 0.81	+0.23 ± 0.61	+0.17 ± 0.60	+0.62 ± 0.89	+0.41 ± 0.74	+0.05 ± 0.52	-0.04 ± 0.74	+0.35 ± 0.06
H11(1600)_HC SSST$_{model}$ anomaly (°C)	+0.94 ± 0.72	+1.11 ± 0.92	+0.49 ± 0.84	+0.77 ± 0.63	+0.55 ± 0.66	+1.34 ± 0.84	+0.73 ± 1.00	+0.45 ± 0.54	+0.39 ± 0.73	+0.75 ± 0.09
September SIC$_{proxy}$	0.19 ± 0.09	0.23 ± 0.09	0.22 ± 0.09	0.13 ± 0.09	0.11 ± 0.09	0.19 ± 0.09	0.63 ± 0.09	0.34 ± 0.09	0.62 ± 0.09	0.30 ± 0.03
LIG_HG September SIC$_{model}$	0.00 ± 0.00	0.71 ± 0.62	0.89 ± 0.32	0.00 ± 0.00	0.67 ± 0.58	0.93 ± 0.12	0.93 ± 0.08	0.73 ± 0.58	0.96 ± 0.02	0.65 ± 0.13
H11(250)_HG September SIC$_{model}$	0.00 ± 0.00	0.79 ± 0.44	0.94 ± 0.10	0.01 ± 0.06	0.80 ± 0.42	0.94 ± 0.10	0.94 ± 0.06	0.85 ± 0.34	0.95 ± 0.02	0.69 ± 0.14
H11(250)_HC September SIC$_{model}$	0.00 ± 0.03	0.42 ± 0.28	0.42 ± 0.32	0.66 ± 0.32	0.96 ± 0.02	0.94 ± 0.13	0.95 ± 0.09	0.47 ± 0.36	0.97 ± 0.00	0.64 ± 0.10
H11(1600)_HC September SIC$_{model}$	0.00 ± 0.03	0.22 ± 0.25	0.22 ± 0.28	0.17 ± 0.35	0.94 ± 0.02	0.93 ± 0.13	0.94 ± 0.09	0.19 ± 0.33	0.97 ± 0.01	0.51 ± 0.16

Table 1: Diatom transfer function values and model output for Peak MIS 5e September SICs$_{model/proxy}$ and SSST$_{model/proxy}$ anomalies (Peak MIS 5e – PI) for nine marine sediment core locations and an average for the SO from the model/proxy values at the nine core sites. Diatom transfer function values for Peak MIS 5e are an average of the 130-128 ka interval and are presented in Chadwick et al. (2022a). For the model output, pink shading indicates conditions that are warmer/have less sea ice than the proxy values, blue shading indicates conditions that are colder/have more sea ice, and no shading indicates conditions that match the proxy values within uncertainty. The errors on the proxy data for each core are the RMSEP values for the diatom transfer function (section 2.2) and the errors on the model data at each core site are two standard deviations for the September SICs and one standard deviation for the SSST anomalies (cf. Guarino et al. 2020).

3.3.   *September SICs_model*

The patterns of September $SICs_{model}$ are very similar between the HadGEM3 simulations (Figure 2a & b), with the main difference a greater $WSIE_{model}$ in the H11(250)_HG run in the Pacific sector region 150-120 °W and in the Weddell Sea to the east of the Antarctic Peninsula (Figure 2b). The HadCM3 simulations both have a reduced $WSIE_{model}$ compared to the HadGEM3 runs, most notably in the eastern Weddell Sea (30 °W – 30 °E) where the WSI edge is >5 ° latitude further south than either of the HadGEM3 runs (Figure 2c & d). In the H11(1600)_HC run, the September $SICs_{model}$ are reduced

Figure 2: Maps of September $SICs_{model}$ for Peak MIS 5e. **A -** LIG_HG. **B** - H11(250)_HG. **C** - H11(250)_HC. **D** - H11(1600)_HC. Coloured circles on all maps represent the September $SICs_{proxy}$ in Chadwick et al. (2022a). The grey line on all maps marks the modern (1981-2010) median September sea-ice extent (Fetterer et al. 2017) and the dashed black lines mark the boundaries between the three SO sectors.

175   compared to H11(250)_HC run, with the WSI edge 2-5 $^\circ$ latitude further poleward in the former (Figure

176   2d).

3.4. September SICs$_{proxy}$

178   Within the ±0.09 uncertainty on the transfer function September SIC$_{proxy}$ values and two standard

179   deviations of the model outputs, the Peak MIS 5e September SICs$_{proxy}$ for many of the cores (TPC290,

180   MD03-2603, U1361A and ANTA91-8) do not match any of the model runs (Table 1 & Figure 2). The

181   match between model and proxy September SICs in the other cores is largely due to the high standard

182   deviations of the model output. The proxy data in cores TPC288, TPC287, ELT17-9 and PC509 are the

183   closest match for the H11(1600)_HC simulation (Table 1). The pattern of September SICs$_{model}$ in the

184   H11(1600)_HC simulation is also the best match with the transfer function values in the sediment

185   cores (Figure 2d), with the greatest discrepancy evident in the expansion of western Pacific sector (150

186    $^\circ$E – 150 $^\circ$W) WSIE$_{model}$, relative to the modern, in the H11(1600)_HC run, compared with the WSIE$_{proxy}$

187   reduction evident in the sediment core data (Figure 2d).

4. Discussion

4.1. SSST$_{model/proxy}$ anomalies

190   For the Pacific sector core sites, the best model-data match for SSST$_{model/proxy}$ anomalies is with the

191   H11(1600)_HC run (Table 1 & Figure 1d), suggesting that the region south of 60 $^\circ$S in this sector was

192   largely 0.5-1 $^\circ$C warmer than PI during Peak MIS 5e (Figure 1d). This SSST$_{model}$ anomaly is consistent

193   with the more southerly SO core sites in Capron et al. (2017) and Chadwick et al. (2020) and suggests

194   that the region south of the APF warmed less than the rest of the SO during MIS 5e. The better match

195   between the proxy data and the H11(1600)_HC simulation than between the proxy data and the

196   H11(250)_HC simulation supports the need to run meltwater-hosed simulations for a longer duration

197   than the 250 years in both the H11(250)_HG and H11(250)_HC runs.

198   In the Indian sector, all the model runs in this study indicate warmer conditions at core site MD03-

199   2603 than the nearby U1361A (Table 1), but none of them have a difference of more than 0.8 $^\circ$C,

200   whereas the transfer function SSST$_{proxy}$ anomalies are >3 $^\circ$C warmer at core site MD03-2603 than

201   U1361A (Table 1). The colder conditions around core U1361A could be due to increased melting of

202   the Wilkes subglacial basin during MIS 5e (Wilson et al. 2018). The shelf bathymetry would likely funnel

203   any colder glacial meltwaters towards U1361A rather than MD03-2603, promoting the difference in

204   SSST$_{model/proxy}$ anomalies. However, this does not explain why the SSST$_{proxy}$ anomaly for core MD03-

205   2603 is still >2 $^\circ$C greater than any of the model results.

206 None of the model runs considered here are able to recreate the ~2.7 °C SSST$_{proxy}$ anomaly in the

207 Atlantic sector cores TPC288 and TPC287 (Table 1 & Figure 1). This discrepancy could be as a result of

208 a poleward constriction of the northern limb of the Weddell Gyre not materialising in the model runs.

209 A constriction of the Weddell Gyre would displace warm (>1.5 °C) surface waters to the south during

210 Peak MIS 5e, causing larger positive SSST$_{proxy}$ anomalies at cores TPC288 and TPC287 than if both cores

211 had remained bathed by Weddell Sea surface waters during Peak MIS 5e. A CMIP3 and CMIP5 model

212 ensemble by Wang (2013) identified that subpolar gyre areal extent displays a diverse response to

213 warmer-than-present climatic conditions, with trends varying from a 23 x 10^{10} m^2/decade decrease to

214 a 69 x 10^{10} m^2/decade increase between models. Our proxy-model comparison could further highlight

215 the deficiencies of subpolar gyre evolution in models, with the greatest discrepancies for the core sites

216 at the edges of the present-day gyre extents.

217 The >2 °C SSST$_{proxy}$ anomalies in cores TPC288, TPC287 and MD03-2603 are greater than other

218 published SSST$_{proxy}$ anomalies from the region south of the APF (Capron et al. 2017, Chadwick et al.

219 2020) and contrasts with the pattern of decreased SSST$_{proxy}$ anomalies towards the continent. The

220 largest SSST$_{proxy}$ anomalies in the Capron et al. (2017) and Chadwick et al. (2020) syntheses were found

221 in cores that were likely bathed by different surface water masses during MIS 5e compared to

222 present/PI (Chadwick et al. 2020), indicating that this is likely also the case for core sites TPC288,

223 TPC287 and MD03-2603. This difference in the surface water mass above the core sites was caused

224 by either changes in gyre extent, in the case of cores TPC288 and TPC287, or by movement of Antarctic

225 Circumpolar Current fronts, in the case of core MD03-2603 (Chadwick et al. 2022a). Comparing the

226 SSST$_{proxy}$ anomalies in the Atlantic and Indian sectors with the Pacific sector shows that there is strong

227 longitudinal heterogeneity in SSST$_{proxy}$ anomalies in addition to the latitudinal variation identified by

228 Chadwick et al. (2020).

229 For the SO south of the APF, Capron et al. (2017) reconstructed a mean SSST$_{proxy}$ anomaly of +1.4 ± 1.2

230 °C during Peak MIS 5e relative to the PI and Chadwick et al. (2022a) reconstructed a mean SSST$_{proxy}$

231 anomaly of +1.6 ± 1.2 °C relative to the PI. Combining these syntheses indicates that the SO south of

232 the APF averaged 1.5 ± 1.2 °C warmer during Peak MIS 5e than the PI.

233 ### *4.2.   September SICs$_{model/proxy}$*

234 In the western Pacific (Ross Sea) sector all the model runs appear to overestimate Peak MIS 5e

235 WSIE$_{model}$, with the HadCM3 runs even indicating an expansion in WSIE$_{model}$ relative to the modern

236 (Figure 2c & d). The eastern Pacific sector has better model-data agreement, especially for the

237 H11(250)_HG and H11(1600)_HC runs (Figure 2b & d). The shape of modern Pacific sector WSIE is

238 strongly influenced by the position of the APF and the shape and position of the Ross Sea Gyre (Nghiem

et al. 2016), with the proxy data indicating a poleward movement of the APF and contraction of the Ross Sea Gyre in the western Pacific sector which is less apparent in the models.

A similar poleward contraction of the Weddell Gyre during MIS 5e, as previously hypothesised with the $SSST_{proxy}$ anomalies in cores TPC288 and TPC287 (section 4.1), would also help explain the shape of the $WSIE_{model}$ in the HadCM3 runs (Figure 2c & d), with a longitudinal constriction of the Weddell Gyre during MIS 5e also supported by proxy data from the western Indian sector (Ghadi et al. 2020). The shape of the eastern Indian sector $WSIE_{model}$ in the HadCM3 simulations in the proximity of cores MD03-2603 and U1361A (Figure 2c & d) is consistent with the greater Peak MIS 5e September SIC_{proxy} reconstructed for core U1361A. High glacial meltwater flux can promote increased WSIE (Merino et al. 2018) and the configuration of the eastern Indian sector WSIE therefore supports a large release of glacial meltwater from the Wilkes subglacial basin during MIS 5e (Wilson et al. 2018), which was channelled towards core U1361A rather than core MD03-2603, as discussed in section 4.1. Many of the estimates of Peak MIS 5e September SIC_{proxy} have a good visual similarity to the models (Figure 2) but do not match the models within the transfer function uncertainty (Table 1). This discrepancy is due to the steep gradient in SIC fraction, with values between 0.2 and 0.8 occupying only a small geographic area (Figure 3), and therefore small variations in the position of the WSI edge can make a large difference to the Peak MIS 5e September $SIC_{model/proxy}$ at most of the core sites. This is supported by the high standard deviation of model output for September $SICs_{model}$ between 0.2 and 0.8 (Table 1).

5. <u>Conclusions</u>

Reconstructed Peak MIS 5e September $SICs_{proxy}$ and $SSST_{proxy}$ anomalies display variation both within and between SO sectors (Figures 1 & 2). The greatest discrepancies between the proxy data and the simulation results are for the WSIE in the western Pacific sector and the SSSTs in the Atlantic sector (Figures 1 & 2), suggested to be due to a poleward contraction of the Ross and Weddell Gyres, respectively, which are seemingly not fully realised in the models.

Of the four HadGEM3 and HadCM3 simulations presented in this study, the best match to the proxy data is provided by the H11(1600)_HC simulation (Figure 1d, Figure 2d & Table 1). The better model-data agreement for the H11(1600)_HC run than for the H11(250)_HC run supports the importance of including North Atlantic meltwater hosing in models of Peak MIS 5e climate and running the models for longer than 250 years. The short run length of the H11(250)_HG simulation explains the poor match to the proxy data as the output is more likely reflective of the conditions at ~133 ka (Marino et al. 2015, Holloway et al. 2018) than 130-128 ka.

271 Running the meltwater hosed H11(250)_HG simulation for a longer duration, ideally 3-4 ka (Marino et

272 al. 2015), is crucial for investigating how well the latest simulations match with the Peak MIS 5e

273 conditions reconstructed from marine sediment cores. Whilst the existing evidence suggests that H11

274 meltwater forcing is required to get a match between the models and proxy data, the current model

275 run-duration is too short and likely needs to be run for at least 1500 years for us to know whether

276 state of the art models are capable of matching the Peak MIS 5e conditions evidenced by the proxy

277 data. Of particular interest in the analysis of longer HadGEM3 runs would be to assess whether the

278 model would resolve the greater reduction in the Atlantic sector $WSIE_{model/proxy}$ seen in both sediment

279 core data (Chadwick et al. 2022a, b) and previous models (Holloway et al. 2017, Holloway et al. 2018)

280 but absent from either the LIG_HG or H11(250)_HG simulations (Figure 2a & b). Additionally, for future

281 model runs there potentially needs to be additional focus on how the Weddell Sea and Ross Sea gyres

282 are realised in the simulations.

283 **Open Research**

284 The MIS 5e September SIC and SSST data for the nine marine sediment cores, produced using the

285 Modern Analog Technique, are available from PANGAEA (https://doi.org/10.1594/PANGAEA.936573)

286 (Chadwick et al. 2021). All HadGEM3 and HadCM3 model output presented in this manuscript are

287 available as netCDF files from the JASMIN group workspace web access site (https://gws-

288 access.jasmin.ac.uk/public/pmip4/EPSL_Chadwicketal_2022/) and will be deposited in Mendeley by

289 the time the article is accepted. Additionally the PI HadGEM3 output is available from the Earth System

290 Grid Federation (https://doi.org/10.22033/ESGF/CMIP6.419) (Ridley et al. 2018a).

291 **Author Contributions**

292 MC – Data curation, Formal analysis, Investigation, Methodology, Resources, Visualisation, Writing –

293 original draft; LCS – Conceptualisation, Funding acquisition, Project administration, Supervision,

294 Writing – review & editing; CSA – Conceptualisation, Funding acquisition, Methodology, Project

295 administration, Resources, Supervision, Writing – review & editing; MVG – Data curation, Formal

296 analysis, Investigation, Methodology, Software, Supervision, Writing – review & editing.

297 **Competing interests**

298 The authors declare they have no competing interests.

299 **Funding**

Acknowledgements

References

312 Abernathey R.P., Cerovecki I., Holland P.R., Newsom E., Mazloff M. & Talley L.D. 2016. Water-mass
313 transformation by sea ice in the upper branch of the Southern Ocean overturning. *Nature Geoscience*,
314 **9** (8): 596-601.

315 Capron E., Govin A., Feng R., Otto-Bliesner B.L. & Wolff E.W. 2017. Critical evaluation of climate
316 syntheses to benchmark CMIP6/PMIP4 127 ka Last Interglacial simulations in the high-latitude regions.
317 *Quaternary Science Reviews*, **168**: 137-150.

318 Chadwick M., Allen C.S. & Crosta X. 2021. MAT estimates of MIS 5e September sea-ice concentrations
319 and summer SSTs. *PANGAEA*.

320 Chadwick M., Allen C.S., Sime L.C., Crosta X. & Hillenbrand C.-D. 2022a. Reconstructing Antarctic
321 winter sea-ice extent during Marine Isotope Stage 5e. *Climate of the Past*, **18**: 129-146.

322 Chadwick M., Allen C.S., Sime L.C., Crosta X. & Hillenbrand C.-D. 2022b. How does the Southern Ocean
323 palaeoenvironment during Marine Isotope Stage 5e compare to the modern? *Marine
324 Micropaleontology*, **170**: 102066.

325 Chadwick M., Allen C.S., Sime L.C. & Hillenbrand C.D. 2020. Analysing the timing of peak warming and
326 minimum winter sea-ice extent in the Southern Ocean during MIS 5e. *Quaternary Science Reviews*,
327 **229**: 106134.

328 Dotto T.S., Naveira Garabato A., Bacon S., Tsamados M., Holland P.R., Hooley J., Frajka-Williams E.,
329 Ridout A. & Meredith M.P. 2018. Variability of the Ross Gyre, Southern Ocean: Drivers and Responses
330 Revealed by Satellite Altimetry. *Geophysical Research Letters*, **45**: 6195-6204.

331 Dyer B., Austermann J., D'Andrea W.J. & Raymo M.E. 2021. Sea-level trends across The Bahamas
332 constrain peak last interglacial ice melt. *PNAS*, **118** (33): e2026839118.

333 Dutton A., Carlson A.E., Long A.J., Milne G.A., Clark P.U., DeConto R., Horton B.P., Rahmstorf S. &
334 Raymo M.E. 2015. Sea-level rise due to polar ice-sheet mass loss during past warm periods. *Science*,
335 **349** (6244): aaa4019.

336 Fetterer F., Knowles K., Meier W.N., Savoie M. & Windnagel A.K. 2017. Sea Ice Index, Version 3.
337 *Boulder, Colorado USA*. NSIDC: National Snow and Ice Data Center.

338 Fischer H., Meissner K.J., Mix A.C., Abram N.J., Austermann J., Brovkin V., Capron E., Colombaroli D.,
339 Daniau A.-L., Dyez K.A., Felis T., Finkelstein S.A., Jaccard S.L., McClymont E.L., Rovere A., Sutter J., Wolff

E.W., Affolter S., Bakker P., Ballesteros-Cánovas J.A., Barbante C., Caley T., Carlson A.E., Churakova O., Cortese G., Cumming B.F., Davis B.A.S., de Vernal A., Emile-Geay J., Fritz S.C. et al. 2018. Palaeoclimate constraints on the impact of 2 °C anthropogenic warming and beyond. *Nature Geoscience*, **11** (7): 474-485.

Ghadi P., Nair A., Crosta X., Mohan R., Manoj M.C. & Meloth T. 2020. Antarctic sea-ice and palaeoproductivity variation over the last 156,000 years in the Indian sector of Southern Ocean. *Marine Micropaleontology*, **160**: 101894.

Guarino M.-V., Sime L.C., Schröeder D., Malmierca-Vallet I., Rosenblum E., Ringer M., Ridley J., Feltham D., Bitz C., Steig E.J., Wolff E., Stroeve J. & Sellar A. 2020. Sea-ice-free Arctic during the Last Interglacial supports fast future loss. *Nature Climate Change*, **10** (10): 928-932.

Guarino M.V., Sime L.C., Schroeder D. & Ridley J. 2022, *in review*. The first 250 years of the Heinrich 11 iceberg discharge: Last Interglacial HadGEM3-GC3.1 simulations for CMIP6-PMIP4. *Climate of the Past Discussions [preprint]*. (https://cp.copernicus.org/preprints/cp-2021-187/).

Hall A. 2004. The Role of Surface Albedo Feedback in Climate. *Journal of Climate*, **17**: 1550-1568.

Hobbs W.R., Massom R., Stammerjohn S., Reid P., Williams G. & Meier W. 2016. A review of recent changes in Southern Ocean sea ice, their drivers and forcings. *Global and Planetary Change*, **143**: 228-250.

Holloway M.D., Sime L.C., Allen C.S., Hillenbrand C.-D., Bunch P., Wolff E. & Valdes P.J. 2017. The spatial structure of the 128 ka Antarctic sea ice minimum. *Geophysical Research Letters*, **44** (21): 11129-11139.

Holloway M.D., Sime L.C., Singarayer J.S., Tindall J.C. & Valdes P.J. 2018. Simulating the 128-ka Antarctic Climate Response to Northern Hemisphere Ice Sheet Melting Using the Isotope-Enabled HadCM3. *Geophysical Research Letters*, **45** (21): 11921-11929.

Madec G., Bourdalle-Badie R., Chanut J., Clementi E., Coward A., Ethe C., Iovino D., Lea D., Levy C., Lovato T., Martin N., Masson S., Mocavero S., Rousset C., Storkey D., Vancoppenolle M., Mueller S., Nurser G., Bell M. & Samson G. 2019. *NEMO ocean engine*: Notes Du Pole De Modelisation De L'institut Pierre-simon Laplace (IPSL).

Maksym T. 2019. Arctic and Antarctic Sea Ice Change: Contrasts, Commonalities, and Causes. *Ann Rev Mar Sci*, **11**: 187-213.

Marino G., Rohling E.J., Rodriguez-Sanz L., Grant K.M., Heslop D., Roberts A.P., Stanford J.D. & Yu J. 2015. Bipolar seesaw control on last interglacial sea level. *Nature*, **522** (7555): 197-201.

Menary M.B., Kuhlbrodt T., Ridley J., Andrews M.B., Dimdore-Miles O.B., Deshayes J., Eade R., Gray L., Ineson S., Mignot J., Roberts C.D., Robson J., Wood R.A. & Xavier P. 2018. Preindustrial Control Simulations With HadGEM3-GC3.1 for CMIP6. *Journal of Advances in Modeling Earth Systems*, **10**: 3049-3075.

Meredith M., Sommerkorn M., Cassotta S., Derksen C., Ekaykin A., Hollowed A., Kofinas G., Mackintosh A., Melbourne-Thomas J., Muelbert M.M.C., Ottersen G., Pritchard H. & Schuur E.A.G. 2019. Polar Regions. In: *IPCC Special Report on the Ocean and Cryosphere in a Changing Climate*, Portner H.O., Roberts D.C., Masson-Delmotte V. et al. Eds. Cambridge University Press**:** 203-320.

Merino N., Jourdain N.C., Le Sommer J., Goosse H., Mathiot P. & Durand G. 2018. Impact of increasing antarctic glacial freshwater release on regional sea-ice cover in the Southern Ocean. *Ocean Modelling*, **121**: 76-89.

382 Nghiem S.V., Rigor I.G., Clemente-Colón P., Neumann G. & Li P.P. 2016. Geophysical constraints on the
383 Antarctic sea ice cover. *Remote Sensing of Environment*, **181**: 281-292.

384 Otto-Bliesner B.L., Braconnot P., Harrison S.P., Lunt D.J., Abe-Ouchi A., Albani S., Bartlein P.J., Capron
385 E., Carlson A.E., Dutton A., Fischer H., Goelzer H., Govin A., Haywood A., Joos F., LeGrande A.N.,
386 Lipscomb W.H., Lohmann G., Mahowald N., Nehrbass-Ahles C., Pausata F.S.R., Peterschmitt J.-Y.,
387 Phipps S.J., Renssen H. & Zhang Q. 2017. The PMIP4 contribution to CMIP6 – Part 2: Two interglacials,
388 scientific objective and experimental design for Holocene and Last Interglacial simulations.
389 *Geoscientific Model Development*, **10** (11): 3979-4003.

390 Otto-Bliesner B.L., Brady E.C., Zhao A., Brierley C., Axford Y., Capron E., Govin A., Hoffman J., Isaacs E.,
391 Kageyama M., Scussolini P., Tzedakis P.C., Williams C., Wolff E., Abe-Ouchi A., Braconnot P., Ramos
392 Buarque S., Cao J., de Vernal A., Guarino M.V., Guo C., LeGrande A.N., Lohmann G., Meissner K.,
393 Menviel L., Nisancioglu K., O'Ishi R., Salas Y Melia D., Shi X., Sicard M. et al. 2021. Large-scale features
394 of Last Interglacial climate: results from evaluating the *lig127k* simulations for the Coupled Model
395 Intercomparison Project (CMIP6)-Paleoclimate Modeling Intercomparison Project (PMIP4). *Climate of*
396 *the Past*, **17**: 63-94.

397 Purich A., England M.H., Cai W., Chikamoto Y., Timmermann A., Fyfe J.C., Frankcombe L., Meehl G.A.
398 & Arblaster J.M. 2016. Tropical Pacific SST Drivers of Recent Antarctic Sea Ice Trends. *Journal of*
399 *Climate*, **29** (24): 8931-8948.

400 Rayner N.A., Parker D.E., Horton E.B., Folland C.K., Alexander L.V., Rowell D.P., Kent E.C. & Kaplan A.
401 2003. Global analyses of sea surface temperature, sea ice, and night marine air temperature since the
402 late nineteenth century. *Journal of Geophysical Research*, **108** (D14): 4407.

403 Ridley J., Menary M.B., Kuhlbrodt T., Andrews M.B. & Andrews T. 2018a. MOHC HadGEM3-GC31-LL
404 model output prepared for CMIP6 CMIP. *Earth System Grid Federation*.

405 Ridley J.K., Blockley E.W., Keen A.B., Rae J.G.L., West A.E. & Schroeder D. 2018b. The sea ice model
406 component of HadGEM3-GC3.1. *Geoscientific Model Development*, **11** (2): 713-723.

407 Rintoul S.R. 2018. The global influence of localized dynamics in the Southern Ocean. *Nature*, **558**
408 (7709): 209-218.

409 Rosenblum E. & Eisenman I. 2017. Sea Ice Trends in Climate Models Only Accurate in Runs with Biased
410 Global Warming. *Journal of Climate*, **30** (16): 6265-6278.

411 Sime L.C., Wolff E.W., Oliver K.I. & Tindall J.C. 2009. Evidence for warmer interglacials in East Antarctic
412 ice cores. *Nature*, **462** (7271): 342-345.

413 Stone E.J., Capron E., Lunt D.J., Payne A.J., Singarayer J.S., Valdes P.J. & Wolff E.W. 2016. Impact of
414 meltwater on high-latitude early Last Interglacial climate. *Climate of the Past*, **12** (9): 1919-1932.

415 Vernet M., Geibert W., Hoppema M., Brown P.J., Haas C., Hellmer H.H., Jokat W., Jullion L., Mazloff
416 M., Bakker D.C.E., Brearley J.A., Croot P., Hattermann T., Hauck J., Hillenbrand C.D., Hoppe C.J.M.,
417 Huhn O., Koch B.P., Lechtenfeld O.J., Meredith M.P., Naveira Garabato A.C., Nöthig E.M., Peeken I.,
418 Rutgers van der Loeff M.M., Schmidtko S., Schröder M., Strass V.H., Torres-Valdés S. & Verdy A. 2019.
419 The Weddell Gyre, Southern Ocean: Present Knowledge and Future Challenges. *Reviews of*
420 *Geophysics*, **57** (3): 623-708.

421 Walters D., Boutle I., Brooks M., Melvin T., Stratton R., Vosper S., Wells H., Williams K., Wood N., Allen
422 T., Bushell A., Copsey D., Earnshaw P., Edwards J., Gross M., Hardiman S., Harris C., Heming J.,
423 Klingaman N., Levine R., Manners J., Martin G., Milton S., Mittermaier M., Morcrette C., Riddick T.,
424 Roberts M., Sanchez C., Selwood P., Stirling A. et al. 2017. The Met Office Unified Model Global

425   Atmosphere 6.0/6.1 and JULES Global Land 6.0/6.1 configurations. *Geoscientific Model Development*,
426   **10** (4): 1487-1520.

427   Wang Z. 2013. On the response of Southern Hemisphere subpolar gyres to climate change in coupled
428   climate models. *Journal of Geophysical Research: Oceans*, **118** (3): 1070-1086.

429   Wilson D.J., Bertram R.A., Needham E.F., van de Flierdt T., Welsh K.J., McKay R.M., Mazumder A.,
430   Riesselman C.R., Jimenez-Espejo F.J. & Escutia C. 2018. Ice loss from the East Antarctic Ice Sheet during
431   late Pleistocene interglacials. *Nature*, **561** (7723): 383-386.

1 **Model-data comparison of Antarctic winter sea-ice extent and Southern**

2 **Ocean sea-surface temperatures during Marine Isotope Stage 5e**

3 M. Chadwick[1,2*]; L.C. Sime[1]; C.S. Allen[1] & M.-V. Guarino[1,3]

4 *[1.] British Antarctic Survey, Cambridge, UK*

5 *[2.] Ocean and Earth Science, University of Southampton, Southampton, UK*

6 *[3.] Earth System Physics Section, International Centre for Theoretical Physics, Trieste, Italy*

7 *Corresponding author:* m.chadwick@cornwall-insight.com, British Antarctic Survey, High Cross, Madingley Rd.,
8 CB3 0ET, Cambridge, UK

9 **Key points**

10 - Different areas of the Southern Ocean show different consistency between model simulations
11   and proxy data.
12 - Inclusion of Heinrich 11 meltwater forcing improves the match between model simulations
13   and proxy data.

14 **Abstract**

15 Marine Isotope Stage (MIS) 5e (130-116 ka) represents a 'process analogue' for future anthropogenic

16 warming. Climate model simulations for MIS 5e have previously failed to produce Southern Ocean

17 sea-surface temperatures (SST) and sea-ice extent reconstructed from marine sediment core proxy

18 records. Here we compare state of the art HadGEM3 and HadCM3 simulations of Peak MIS 5e

19 Southern Ocean summer SST and September sea-ice concentrations with the latest marine sediment

20 core proxy data. The model outputs and proxy records show the least consistency in the regions

21 located near the present-day Southern Ocean gyre boundaries, implying that model simulations are

22 currently unable to fully realise changes in gyre extent and position during MIS 5e. Including Heinrich

23 11 meltwater forcing in Peak MIS 5e climate simulations improves the likeness to proxy data but it is

24 clear that longer (3-4 ka) run times are required to fully test the consistency between models and

25 data.

26 **Plain Language Summary**

27 Investigating past warm periods can provide us with an analogue for how climate will respond to

28 future warming. In this study we compare the latest computer simulations of Southern Ocean sea-

29 surface temperatures and Antarctic winter sea-ice extent from 130,000 years ago with data from

30 marine sediment cores. The simulations and sediment core data show the least match in the areas

31 near the boundaries of the present day Southern Ocean gyres (large, circulating ocean currents),

32 implying that changes in the position and size of the gyres are not fully recreated in the computer
33 simulations. The inclusion of ice sheet meltwater into the North Atlantic improves the comparison
34 between the simulations and sediment core data but it is clear that longer simulation run times are
35 required to fully test their consistency.

36 **Keywords**

37 Last interglacial; Southern Ocean; sea ice; sea-surface temperatures; model-data comparison

38 **1. Introduction**

39 In the present day, Antarctic winter sea ice covers an area of ~1.8 x 10^6 km^2 and forms a critical
40 component of the global climate system (Maksym 2019). Sea ice has a high albedo or 'reflectivity' (Hall
41 2004), and seasonal growth in sea ice influences the strength of Southern Ocean (SO) and global
42 overturning circulation through the formation of dense Antarctic shelf and bottom waters
43 (Abernathey et al. 2016, Rintoul 2018). Rising atmospheric greenhouse gas concentrations are driving
44 current global warming, with a predicted reduction of 24-34 % in the Antarctic winter sea-ice extent
45 (WSIE) by 2100 (Meredith et al. 2019). The short length of the observational record for Antarctic sea
46 ice, coupled with the complex climate dynamics involved in changes to modern WSIE (Hobbs et al.
47 2016, Purich et al. 2016) mean that model simulations have been unable to faithfully replicate recent
48 changes in Antarctic sea ice unless they use unrealistically reduced warming (Rosenblum & Eisenman
49 2017). Marine Isotope Stage (MIS) 5e proxy records offer valuable evidence of a 'warmer-than-
50 present' climate, and the opportunity to improve our understanding/prediction of the impacts of
51 future climate change.

52 During MIS 5e (130-116 ka) both mean annual global atmospheric temperatures and mean annual SO
53 sea-surface temperatures (SSTs) peaked at ~2 ^{o}C warmer than preindustrial (PI) (Capron et al. 2017,
54 Fischer et al. 2018). Global sea levels were also 1.2-5.3 m higher than the present day (Dyer et al.
55 2021). Unlike future anthropogenic warming, MIS 5e warming is forced by orbital changes, alongside
56 a variety of internal ocean-ice-atmosphere feedbacks, rather than being driven by increasing
57 atmospheric greenhouse gas concentrations. However, MIS 5e represents an important 'process
58 analogue' for understanding the climatic mechanisms and feedbacks active under warmer-than-
59 present climates (Stone et al. 2016).

60 Model simulations of the Peak MIS 5e climate at 127 ka are a part of the Coupled Model
61 Intercomparison Project (CMIP6) and Paleoclimate Modelling Intercomparison Project (PMIP4) (Otto-
62 Bliesner et al. 2017). Analysis of the short (50-100 years) orbitally forced CMIP6-PMIP4 ensembles
63 indicate that these simulations exhibit SO summer $SSTs_{model}$ (SSSTs) which were ~0.5 ^{o}C cooler during

64 Peak MIS 5e than the PI and that there was an average reduction of ~5-8 % in WSIE at 127 ka relative

65 to the PI (Otto-Bliesner et al. 2021). These simulation results are a poor match for published Peak MIS

66 5e proxy records from SO marine sediment cores, which indicate a $SSST_{proxy}$ warming of 0-5 °C relative

67 to the PI (Capron et al. 2017, Otto-Bliesner et al. 2021). The SO model-data discrepancy is hypothesised

68 to be due to the absence of the Heinrich 11 (H11) meltwater event in CMIP6-PMIP4 Tier 1 simulations

69 (Otto-Bliesner et al. 2021). Though we also note that model-data comparisons of MIS 5e Antarctic

70 WSIE have been limited by the location of most published marine sediment core records: they are

71 located north of the modern WSIE, and likely also north of the 127 ka WSIE (Holloway et al. 2017,

72 Chadwick et al. 2020).

73 The published syntheses of proxy records from SO marine sediment cores in Capron et al. (2017) and

74 Chadwick et al. (2020) indicate Peak MIS 5e $SSSTs_{proxy}$ were between 0 and 5 °C warmer than the

75 present and PI, with this warming anomaly decreasing towards the South Pole. The most southerly

76 marine cores in these syntheses have $SSST_{proxy}$ anomalies for Peak MIS 5e of <1.5 °C (40 °W – 40 °E),

77 but there are no MIS 5e marine records located south of the modern Antarctic Polar Front (APF) for

78 most of the SO (80 °E – 40 °W).

79 Whilst most proxy records of Antarctic sea ice are located too far north to precisely constrain the Peak

80 MIS 5e $WSIE_{proxy}$, a recent reconstruction suggests that the winter sea-ice (WSI) edge was located 1-2°

81 south of its modern position in the Pacific sector and >5° south of its modern position in the Atlantic

82 sector (Chadwick et al. 2022a).

83 This study presents a new model-data comparison for the Southern Ocean during MIS 5e. Peak MIS

84 5e Antarctic September sea-ice concentrations (SIC_{model}) and SO $SSSTs_{model}$ from the latest UK fully-

85 coupled HadGEM3-GC3.1 (hereafter HadGEM3) numerical simulations, both with and without the H11

86 meltwater event (Guarino et al. 2022, *in review*), and from the H11 meltwater-hosed HadCM3

87 numerical simulations in Holloway et al. (2018) are compared with the latest diatom transfer function

88 estimates of September SIC_{proxy} and $SSSTs_{proxy}$ from nine marine sediment cores (Chadwick et al. 2021,

89 Chadwick et al. 2022a) to answer the following:

90 - Can we now tell if different areas of the Southern Ocean show more or less consistency
91 between model simulations and proxy data during MIS 5e?

92 - Is H11 meltwater forcing necessary for the models to match the proxy records?

93 - Are our current state of the art models capable of simulating the proxy data?

2. **Materials and methods**

2.1. Numerical simulations

HadGEM3 is a global coupled atmosphere-land-ocean-ice model which combines the Unified Model Atmosphere model (Walters et al. 2017), the JULES land surface model (Walters et al. 2017), the NEMO ocean model (Madec et al. 2019) and the CICE sea-ice model (Ridley et al. 2018b). The PI control run is presented in Menary et al. (2018) and uses a constant 1850 climate forcing (see Menary et al. (2018) for further details).

The standard Peak MIS 5e simulation (hereafter referred to as LIG_HG) is published in Guarino et al. (2020) and the H11 simulation is published in Guarino et al. (2022, *in review*). They were run using the protocol described in Otto-Bliesner et al. (2017) for Tier 1 and Tier 2 PMIP4 simulations. The Peak MIS 5e climate was simulated by forcing the HadGEM3 model with constant last interglacial orbital and greenhouse gas boundary conditions (see Guarino et al. (2022, *in review*) for further details). In the H11 run, the H11 meltwater event is simulated by adding a constant freshwater flux equal to 0.2 Sv, evenly across the North Atlantic between 50 and 70 °N (Otto-Bliesner et al. 2017). The H11 simulation was run for 250 years with the climatological averages from the final 100 years (150-250 years) presented here (hereafter referred to as H11(250)_HG).

HadCM3 is a faster running, but older and lower resolution, UK model than HadGEM3. The HadCM3 simulations are published in Holloway et al. (2018), with 0.25 Sv freshwater forcing to the North Atlantic applied for 1600 years. We use the climatological averages for years 150-250 of the model run (hereafter referred to as H11(250)_HC), to match the length of the run performed for HadGEM3, and the last 100 years (1500-1600 years)(hereafter referred to as H11(1600)_HC), to examine how SSSTs$_{model}$ and SICs$_{model}$ evolved after a longer period of H11 type forcing.

MIS 5e SSSTs$_{model}$ (average January to March) are presented as anomalies relative to the PI control runs whereas September SICs$_{model}$ are presented as absolute values.

2.2. Marine sediment cores

Modern Analog Technique diatom transfer function estimates of September SICs$_{proxy}$ and SSSTs$_{proxy}$ for Peak MIS 5e, reconstructed from nine marine sediment cores and published in Chadwick et al. (2022a), are compared to model output. The transfer function methodology is detailed in Chadwick et al. (2022a) and the data for all the cores is available from Chadwick et al. (2021). Reconstructed September SICs$_{proxy}$ have a Root Mean Square Error of Prediction (RMSEP) of 0.09 and SSSTs$_{proxy}$ have a RMSEP of 1.1 °C. For PI SSSTs$_{proxy}$ at each core site the average January-March SST$_{proxy}$ from 1870-1900 was calculated from the HadISST1 dataset (Rayner et al. 2003). The average SSST$_{proxy}$ and

126   September SIC$_{proxy}$ in the 130-128 ka interval is considered to represent Peak MIS 5e conditions. This

127   time interval is chosen as it is within the chronological uncertainty (±2 ka) of both the peak δ^{18}O in the

128   EPICA Dome C ice core record at ~128 ka (Sime et al. 2009) and the termination of the H11 meltwater

129   event at 130 ka (Marino et al. 2015).

130   ## 3. Results

131   ### 3.1. SSST$_{model}$ anomalies

132   In both the LIG_HG and H11(250)_HG simulations the pattern of SSST$_{model}$ anomalies for Peak MIS 5e

133   relative to the PI is very similar (Figure 1a & b). Both runs show a cooling (0-1 °C) in the Atlantic sector

134   (70 °W – 20 °E) and a warming (0-1.5 °C) in the Indian sector (20 – 150 °E) during Peak MIS 5e relative

135   to the PI, with both trends more pronounced in the H11(250)_HG run (Figure 1b). In the Pacific sector

136   (150 °E – 70 °W), both the LIG_HG and H11(250)_HG simulations show a warming (0-1 °C) in the

137   eastern region (120 – 70 °W) and a cooling (0-0.5 °C) in the western region, south of the modern WSIE

138   (150 °E – 150 °W) but have diverging trends in the central area (150 – 120 °W) where the LIG_HG run

139   has a warming of up to 1 °C and the H11(250)_HG run has a mixture of warming and cooling, all by

140   less than 0.5 °C (Figure 1a & b).

141   The H11(250)_HC and H11(1600)_HC simulations both have greater warming trends than either of the

142   HadGEM3 runs, with only a few localised areas of cooling in the H11(250)_HC run and none in

143   H11(1600)_HC run (Figure 1c & d). In the H11(250)_HC run, the area north of the modern WSIE had

144   largely warmed by 0.5-1.5 °C, whereas the region within the modern WSIE was generally less than 0.5

145   °C warmer than PI (Figure 1c). In the H11(1600)_HC run the SSST$_{model}$ anomalies have increased

146   throughout the SO relative to the H11(250)_HC run, with the region within the modern WSIE mainly

147   0.5-1.5 °C warmer than PI and the area to the north of the modern WSIE largely showing 1-3 °C

148   warming (Figure 1d). All simulations show the greatest Peak MIS 5e warming in the 90-170 °E region,

149   north of 60 °S (Figure 1).

150   ### 3.2. SSST$_{proxy}$ anomalies

151   With the exception of core TPC290, the sediment cores all indicate warmer conditions during Peak

152   MIS 5e than the PI (Table 1 & Figure 1). The Pacific sector cores have SSST$_{proxy}$ anomalies of less than

153   1.5 °C, with the more southerly cores showing a warming of less than 1 °C (Table 1). The nearby cores

154   TPC288 and TPC287 in the Atlantic sector have similar SSST$_{proxy}$ anomalies to each other, whereas, in

155   the Indian sector, the proximally located cores MD03-2603 and U1361A have very different SSST$_{proxy}$

156   anomalies to each other, with the SSST$_{proxy}$ anomaly for core MD03-2603 more than 3 °C warmer than

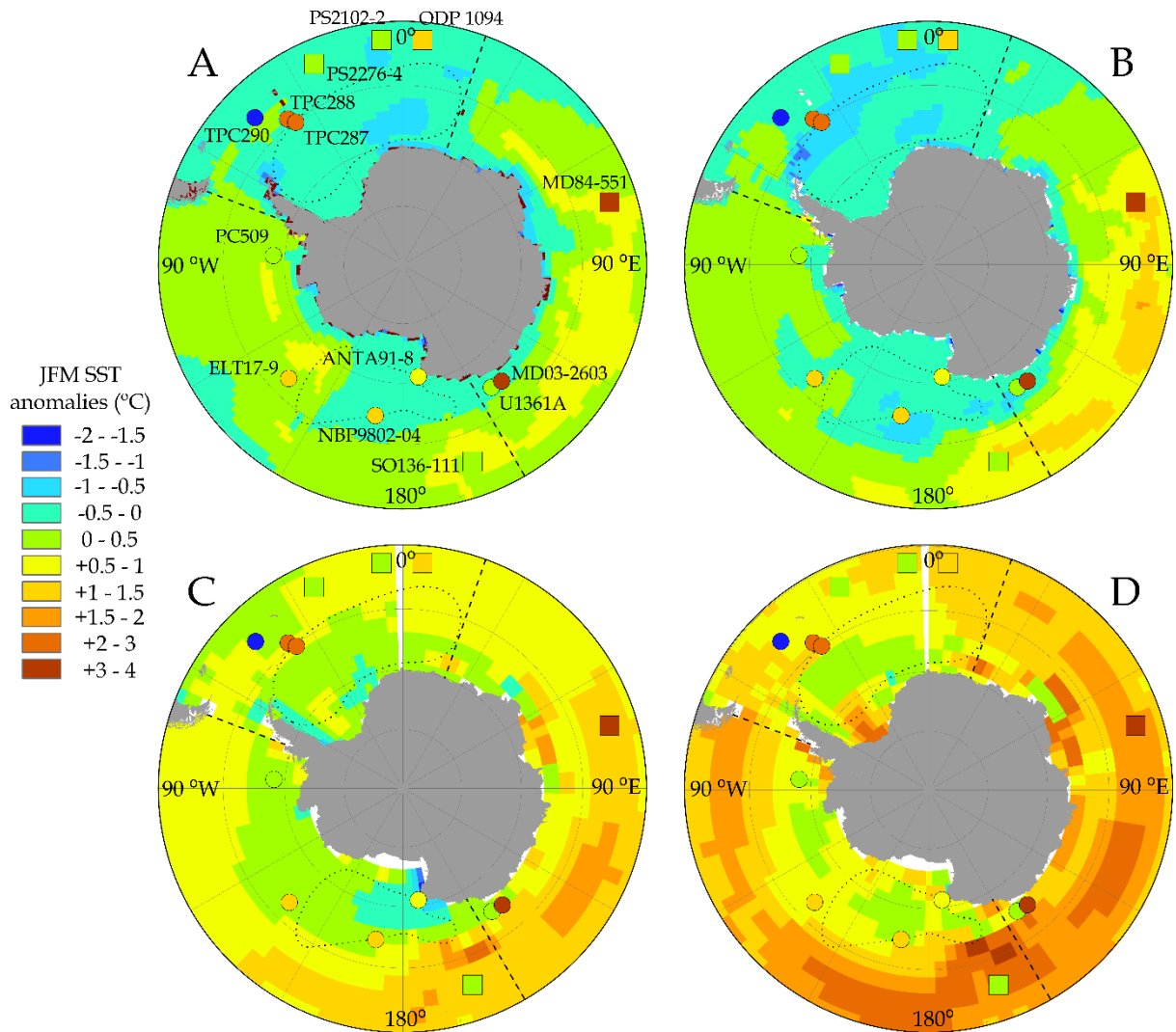157   the anomaly in core U1361A (Table 1 & Figure 1).

Figure 1: Maps of summer (JFM) SST_{model} anomalies for Peak MIS 5e relative to the PI. **A** - LIG_HG. **B** - H11(250)_HG. **C** - H11(250)_HC. **D** - H11(1600)_HC. Coloured circles on all maps represent the JFM SST_{proxy} anomalies from Chadwick et al. (2022a) and coloured squares represent the summer SST_{proxy} anomalies from Capron et al. (2017). The dashed black lines mark the boundaries between the three SO sectors and the dotted black lines mark the modern extents of the Weddell Sea and Ross Sea gyres (positions of the Weddell Sea gyre is from Vernet et al. (2019) and the Ross Sea gyre is from Dotto et al. (2018)).

158 Within the ±1.1 °C uncertainty on the diatom transfer function $SSST_{proxy}$ values and the standard

159 deviation of the model output, the Peak MIS 5e – PI $SSST_{proxy}$ anomalies in all Pacific sector cores match

160 the H11(250)_HC and H11(1600)_HC runs (Table 1, Figure 1c & d). Proxy data for cores PC509 and

161 ANTA91-8 also match the HadGEM3 model outputs (Table 1) and the proxy data in core ELT17-9

162 matches the LIG_HG run (Table 1). The transfer function Peak MIS 5e $SSST_{proxy}$ anomaly in core U1361A

163 also matches, within uncertainty, the values from all four model runs (Table 1). The transfer function

164 $SSST_{proxy}$ anomalies in cores TPC288 and MD03-2603 only match the model output for H11(1600)_HC

165 and in core TPC287 there is not a match with any of the model outputs considered here (Table 1).

166   Cores TPC288, TPC287 and MD03-2603 have SSST$_{proxy}$ anomalies >2 °C warmer than all the models and

167   core TPC290 >1.5 °C cooler than all the models (Table 1).

	TPC290	TPC288	TPC287	ELT17-9	NBP9802-04	MD03-2603	U1361A	PC509	ANTA91-8	SO average (mean ± st. dev.)
Latitude (°S), Longitude (°E)	55.55, -45.02	59.14, -37.96	60.31, -36.65	63.08, -135.12	64.20, -170.08	64.28, 139.38	64.41, 143.89	68.31, -86.03	70.78, 172.83	-
SSST$_{proxy}$ anomaly (°C)	-1.70 ± 1.10	+2.65 ± 1.10	+2.75 ± 1.10	+1.24 ± 1.10	+1.43 ± 1.10	+3.13 ± 1.10	+0.04 ± 1.10	+0.24 ± 1.10	+1.00 ± 1.10	+1.56 ± 1.19
LIG_HG SSST$_{model}$ anomaly (°C)	-0.03 ± 0.67	-0.19 ± 0.90	-0.31 ± 1.02	+0.19 ± 0.91	-0.32 ± 1.06	-0.19 ± 1.05	-0.20 ± 1.18	+0.25 ± 1.01	-0.10 ± 0.29	-0.10 ± 0.04
H11(250)_HG SSST$_{model}$ anomaly (°C)	-0.16 ± 0.60	-0.50 ± 0.90	-0.78 ± 0.92	-0.03 ± 1.11	-0.55 ± 1.00	-0.50 ± 1.07	-0.66 ± 1.17	-0.02 ± 0.83	-0.13 ± 0.26	-0.37 ± 0.07
H11(250)_HC SSST$_{model}$ anomaly (°C)	+0.45 ± 0.72	+0.67 ± 0.82	+0.62 ± 0.81	+0.23 ± 0.61	+0.17 ± 0.60	+0.62 ± 0.89	+0.41 ± 0.74	+0.05 ± 0.52	-0.04 ± 0.74	+0.35 ± 0.06
H11(1600)_HC SSST$_{model}$ anomaly (°C)	+0.94 ± 0.72	+1.11 ± 0.92	+0.49 ± 0.84	+0.77 ± 0.63	+0.55 ± 0.66	+1.34 ± 0.84	+0.73 ± 1.00	+0.45 ± 0.54	+0.39 ± 0.73	+0.75 ± 0.09
September SIC$_{proxy}$	0.19 ± 0.09	0.23 ± 0.09	0.22 ± 0.09	0.13 ± 0.09	0.11 ± 0.09	0.19 ± 0.09	0.63 ± 0.09	0.34 ± 0.09	0.62 ± 0.09	0.30 ± 0.03
LIG_HG September SIC$_{model}$	0.00 ± 0.00	0.71 ± 0.62	0.89 ± 0.32	0.00 ± 0.00	0.67 ± 0.58	0.93 ± 0.12	0.93 ± 0.08	0.73 ± 0.58	0.96 ± 0.02	0.65 ± 0.13
H11(250)_HG September SIC$_{model}$	0.00 ± 0.00	0.79 ± 0.44	0.94 ± 0.10	0.01 ± 0.06	0.80 ± 0.42	0.94 ± 0.10	0.94 ± 0.06	0.85 ± 0.34	0.95 ± 0.02	0.69 ± 0.14
H11(250)_HC September SIC$_{model}$	0.00 ± 0.03	0.42 ± 0.28	0.42 ± 0.32	0.66 ± 0.32	0.96 ± 0.02	0.94 ± 0.13	0.95 ± 0.09	0.47 ± 0.36	0.97 ± 0.00	0.64 ± 0.10
H11(1600)_HC September SIC$_{model}$	0.00 ± 0.03	0.22 ± 0.25	0.22 ± 0.28	0.17 ± 0.35	0.94 ± 0.02	0.93 ± 0.13	0.94 ± 0.09	0.19 ± 0.33	0.97 ± 0.01	0.51 ± 0.16

Table 1: Diatom transfer function values and model output for Peak MIS 5e September SICs$_{model/proxy}$ and SSST$_{model/proxy}$ anomalies (Peak MIS 5e – PI) for nine marine sediment core locations and an average for the SO from the model/proxy values at the nine core sites. Diatom transfer function values for Peak MIS 5e are an average of the 130-128 ka interval and are presented in Chadwick et al. (2022a). For the model output, pink shading indicates conditions that are warmer/have less sea ice than the proxy values, blue shading indicates conditions that are colder/have more sea ice, and no shading indicates conditions that match the proxy values within uncertainty. The errors on the proxy data for each core are the RMSEP values for the diatom transfer function (section 2.2) and the errors on the model data at each core site are two standard deviations for the September SICs and one standard deviation for the SSST anomalies (cf. Guarino et al. 2020).

3.3.   *September SICs_model*

The patterns of September $SICs_{model}$ are very similar between the HadGEM3 simulations (Figure 2a & b), with the main difference a greater $WSIE_{model}$ in the H11(250)_HG run in the Pacific sector region 150-120 °W and in the Weddell Sea to the east of the Antarctic Peninsula (Figure 2b). The HadCM3 simulations both have a reduced $WSIE_{model}$ compared to the HadGEM3 runs, most notably in the eastern Weddell Sea (30 °W – 30 °E) where the WSI edge is >5 ° latitude further south than either of the HadGEM3 runs (Figure 2c & d). In the H11(1600)_HC run, the September $SICs_{model}$ are reduced
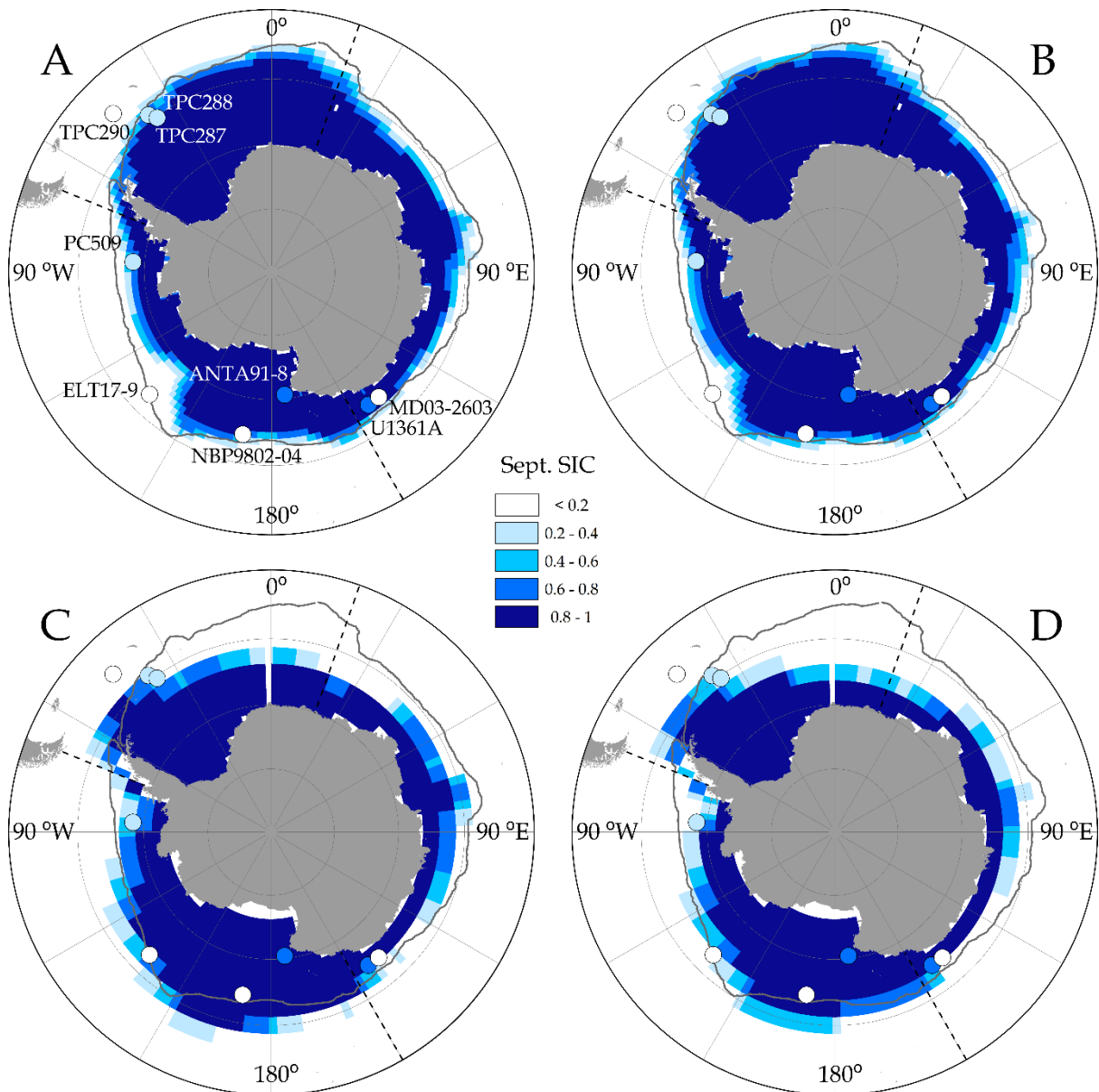

Figure 2: Maps of September $SICs_{model}$ for Peak MIS 5e. **A -** LIG_HG. **B** - H11(250)_HG. **C** - H11(250)_HC. **D** - H11(1600)_HC. Coloured circles on all maps represent the September $SICs_{proxy}$ in Chadwick et al. (2022a). The grey line on all maps marks the modern (1981-2010) median September sea-ice extent (Fetterer et al. 2017) and the dashed black lines mark the boundaries between the three SO sectors.

175   compared to H11(250)_HC run, with the WSI edge 2-5 $^{\circ}$ latitude further poleward in the former (Figure

176   2d).

3.4. September SICs$_{proxy}$

178   Within the ±0.09 uncertainty on the transfer function September SIC$_{proxy}$ values and two standard

179   deviations of the model outputs, the Peak MIS 5e September SICs$_{proxy}$ for many of the cores (TPC290,

180   MD03-2603, U1361A and ANTA91-8) do not match any of the model runs (Table 1 & Figure 2). The

181   match between model and proxy September SICs in the other cores is largely due to the high standard

182   deviations of the model output. The proxy data in cores TPC288, TPC287, ELT17-9 and PC509 are the

183   closest match for the H11(1600)_HC simulation (Table 1). The pattern of September SICs$_{model}$ in the

184   H11(1600)_HC simulation is also the best match with the transfer function values in the sediment

185   cores (Figure 2d), with the greatest discrepancy evident in the expansion of western Pacific sector (150

186     $^{\circ}$E – 150 $^{\circ}$W) WSIE$_{model}$, relative to the modern, in the H11(1600)_HC run, compared with the WSIE$_{proxy}$

187   reduction evident in the sediment core data (Figure 2d).

4. <u>Discussion</u>

4.1. SSST$_{model/proxy}$ anomalies

190   For the Pacific sector core sites, the best model-data match for SSST$_{model/proxy}$ anomalies is with the

191   H11(1600)_HC run (Table 1 & Figure 1d), suggesting that the region south of 60 $^{\circ}$S in this sector was

192   largely 0.5-1 $^{\circ}$C warmer than PI during Peak MIS 5e (Figure 1d). This SSST$_{model}$ anomaly is consistent

193   with the more southerly SO core sites in Capron et al. (2017) and Chadwick et al. (2020) and suggests

194   that the region south of the APF warmed less than the rest of the SO during MIS 5e. The better match

195   between the proxy data and the H11(1600)_HC simulation than between the proxy data and the

196   H11(250)_HC simulation supports the need to run meltwater-hosed simulations for a longer duration

197   than the 250 years in both the H11(250)_HG and H11(250)_HC runs.

198   In the Indian sector, all the model runs in this study indicate warmer conditions at core site MD03-

199   2603 than the nearby U1361A (Table 1), but none of them have a difference of more than 0.8 $^{\circ}$C,

200   whereas the transfer function SSST$_{proxy}$ anomalies are >3 $^{\circ}$C warmer at core site MD03-2603 than

201   U1361A (Table 1). The colder conditions around core U1361A could be due to increased melting of

202   the Wilkes subglacial basin during MIS 5e (Wilson et al. 2018). The shelf bathymetry would likely funnel

203   any colder glacial meltwaters towards U1361A rather than MD03-2603, promoting the difference in

204   SSST$_{model/proxy}$ anomalies. However, this does not explain why the SSST$_{proxy}$ anomaly for core MD03-

205   2603 is still >2 $^{\circ}$C greater than any of the model results.

206   None of the model runs considered here are able to recreate the ~2.7 °C SSST$_{proxy}$ anomaly in the

207   Atlantic sector cores TPC288 and TPC287 (Table 1 & Figure 1). This discrepancy could be as a result of

208   a poleward constriction of the northern limb of the Weddell Gyre not materialising in the model runs.

209   A constriction of the Weddell Gyre would displace warm (>1.5 °C) surface waters to the south during

210   Peak MIS 5e, causing larger positive SSST$_{proxy}$ anomalies at cores TPC288 and TPC287 than if both cores

211   had remained bathed by Weddell Sea surface waters during Peak MIS 5e. A CMIP3 and CMIP5 model

212   ensemble by Wang (2013) identified that subpolar gyre areal extent displays a diverse response to

213   warmer-than-present climatic conditions, with trends varying from a 23 x 10^{10} m^2/decade decrease to

214   a 69 x 10^{10} m^2/decade increase between models. Our proxy-model comparison could further highlight

215   the deficiencies of subpolar gyre evolution in models, with the greatest discrepancies for the core sites

216   at the edges of the present-day gyre extents.

217   The >2 °C SSST$_{proxy}$ anomalies in cores TPC288, TPC287 and MD03-2603 are greater than other

218   published SSST$_{proxy}$ anomalies from the region south of the APF (Capron et al. 2017, Chadwick et al.

219   2020) and contrasts with the pattern of decreased SSST$_{proxy}$ anomalies towards the continent. The

220   largest SSST$_{proxy}$ anomalies in the Capron et al. (2017) and Chadwick et al. (2020) syntheses were found

221   in cores that were likely bathed by different surface water masses during MIS 5e compared to

222   present/PI (Chadwick et al. 2020), indicating that this is likely also the case for core sites TPC288,

223   TPC287 and MD03-2603. This difference in the surface water mass above the core sites was caused

224   by either changes in gyre extent, in the case of cores TPC288 and TPC287, or by movement of Antarctic

225   Circumpolar Current fronts, in the case of core MD03-2603 (Chadwick et al. 2022a). Comparing the

226   SSST$_{proxy}$ anomalies in the Atlantic and Indian sectors with the Pacific sector shows that there is strong

227   longitudinal heterogeneity in SSST$_{proxy}$ anomalies in addition to the latitudinal variation identified by

228   Chadwick et al. (2020).

229   For the SO south of the APF, Capron et al. (2017) reconstructed a mean SSST$_{proxy}$ anomaly of +1.4 ± 1.2

230   °C during Peak MIS 5e relative to the PI and Chadwick et al. (2022a) reconstructed a mean SSST$_{proxy}$

231   anomaly of +1.6 ± 1.2 °C relative to the PI. Combining these syntheses indicates that the SO south of

232   the APF averaged 1.5 ± 1.2 °C warmer during Peak MIS 5e than the PI.

233   ### 4.2.   September SICs$_{model/proxy}$

234   In the western Pacific (Ross Sea) sector all the model runs appear to overestimate Peak MIS 5e

235   WSIE$_{model}$, with the HadCM3 runs even indicating an expansion in WSIE$_{model}$ relative to the modern

236   (Figure 2c & d). The eastern Pacific sector has better model-data agreement, especially for the

237   H11(250)_HG and H11(1600)_HC runs (Figure 2b & d). The shape of modern Pacific sector WSIE is

238   strongly influenced by the position of the APF and the shape and position of the Ross Sea Gyre (Nghiem

239 et al. 2016), with the proxy data indicating a poleward movement of the APF and contraction of the
240 Ross Sea Gyre in the western Pacific sector which is less apparent in the models.

241 A similar poleward contraction of the Weddell Gyre during MIS 5e, as previously hypothesised with
242 the $SSST_{proxy}$ anomalies in cores TPC288 and TPC287 (section 4.1), would also help explain the shape
243 of the $WSIE_{model}$ in the HadCM3 runs (Figure 2c & d), with a longitudinal constriction of the Weddell
244 Gyre during MIS 5e also supported by proxy data from the western Indian sector (Ghadi et al. 2020).
245 The shape of the eastern Indian sector $WSIE_{model}$ in the HadCM3 simulations in the proximity of cores
246 MD03-2603 and U1361A (Figure 2c & d) is consistent with the greater Peak MIS 5e September SIC_{proxy}
247 reconstructed for core U1361A. High glacial meltwater flux can promote increased WSIE (Merino et
248 al. 2018) and the configuration of the eastern Indian sector WSIE therefore supports a large release of
249 glacial meltwater from the Wilkes subglacial basin during MIS 5e (Wilson et al. 2018), which was
250 channelled towards core U1361A rather than core MD03-2603, as discussed in section 4.1. Many of
251 the estimates of Peak MIS 5e September SIC_{proxy} have a good visual similarity to the models (Figure 2)
252 but do not match the models within the transfer function uncertainty (Table 1). This discrepancy is
253 due to the steep gradient in SIC fraction, with values between 0.2 and 0.8 occupying only a small
254 geographic area (Figure 3), and therefore small variations in the position of the WSI edge can make a
255 large difference to the Peak MIS 5e September $SIC_{model/proxy}$ at most of the core sites. This is supported
256 by the high standard deviation of model output for September $SICs_{model}$ between 0.2 and 0.8 (Table
257 1).

5. **Conclusions**

259 Reconstructed Peak MIS 5e September $SICs_{proxy}$ and $SSST_{proxy}$ anomalies display variation both within
260 and between SO sectors (Figures 1 & 2). The greatest discrepancies between the proxy data and the
261 simulation results are for the WSIE in the western Pacific sector and the SSSTs in the Atlantic sector
262 (Figures 1 & 2), suggested to be due to a poleward contraction of the Ross and Weddell Gyres,
263 respectively, which are seemingly not fully realised in the models.

264 Of the four HadGEM3 and HadCM3 simulations presented in this study, the best match to the proxy
265 data is provided by the H11(1600)_HC simulation (Figure 1d, Figure 2d & Table 1). The better model-
266 data agreement for the H11(1600)_HC run than for the H11(250)_HC run supports the importance of
267 including North Atlantic meltwater hosing in models of Peak MIS 5e climate and running the models
268 for longer than 250 years. The short run length of the H11(250)_HG simulation explains the poor
269 match to the proxy data as the output is more likely reflective of the conditions at ~133 ka (Marino et
270 al. 2015, Holloway et al. 2018) than 130-128 ka.

271 Running the meltwater hosed H11(250)_HG simulation for a longer duration, ideally 3-4 ka (Marino et
272 al. 2015), is crucial for investigating how well the latest simulations match with the Peak MIS 5e
273 conditions reconstructed from marine sediment cores. Whilst the existing evidence suggests that H11
274 meltwater forcing is required to get a match between the models and proxy data, the current model
275 run-duration is too short and likely needs to be run for at least 1500 years for us to know whether
276 state of the art models are capable of matching the Peak MIS 5e conditions evidenced by the proxy
277 data. Of particular interest in the analysis of longer HadGEM3 runs would be to assess whether the
278 model would resolve the greater reduction in the Atlantic sector WSIE$_{model/proxy}$ seen in both sediment
279 core data (Chadwick et al. 2022a, b) and previous models (Holloway et al. 2017, Holloway et al. 2018)
280 but absent from either the LIG_HG or H11(250)_HG simulations (Figure 2a & b). Additionally, for future
281 model runs there potentially needs to be additional focus on how the Weddell Sea and Ross Sea gyres
282 are realised in the simulations.

283 **Open Research**

284 The MIS 5e September SIC and SSST data for the nine marine sediment cores, produced using the
285 Modern Analog Technique, are available from PANGAEA (https://doi.org/10.1594/PANGAEA.936573)
286 (Chadwick et al. 2021). All HadGEM3 and HadCM3 model output presented in this manuscript are
287 available as netCDF files from the JASMIN group workspace web access site (https://gws-
288 access.jasmin.ac.uk/public/pmip4/EPSL_Chadwicketal_2022/) and will be deposited in Mendeley by
289 the time the article is accepted. Additionally the PI HadGEM3 output is available from the Earth System
290 Grid Federation (https://doi.org/10.22033/ESGF/CMIP6.419) (Ridley et al. 2018a).

291 **Author Contributions**

292 MC – Data curation, Formal analysis, Investigation, Methodology, Resources, Visualisation, Writing –
293 original draft; LCS – Conceptualisation, Funding acquisition, Project administration, Supervision,
294 Writing – review & editing; CSA – Conceptualisation, Funding acquisition, Methodology, Project
295 administration, Resources, Supervision, Writing – review & editing; MVG – Data curation, Formal
296 analysis, Investigation, Methodology, Software, Supervision, Writing – review & editing.

297 **Competing interests**

298 The authors declare they have no competing interests.

299 **Funding**

References

312 Abernathey R.P., Cerovecki I., Holland P.R., Newsom E., Mazloff M. & Talley L.D. 2016. Water-mass
313 transformation by sea ice in the upper branch of the Southern Ocean overturning. *Nature Geoscience*,
314 **9** (8): 596-601.

315 Capron E., Govin A., Feng R., Otto-Bliesner B.L. & Wolff E.W. 2017. Critical evaluation of climate
316 syntheses to benchmark CMIP6/PMIP4 127 ka Last Interglacial simulations in the high-latitude regions.
317 *Quaternary Science Reviews*, **168**: 137-150.

318 Chadwick M., Allen C.S. & Crosta X. 2021. MAT estimates of MIS 5e September sea-ice concentrations
319 and summer SSTs. *PANGAEA*.

320 Chadwick M., Allen C.S., Sime L.C., Crosta X. & Hillenbrand C.-D. 2022a. Reconstructing Antarctic
321 winter sea-ice extent during Marine Isotope Stage 5e. *Climate of the Past*, **18**: 129-146.

322 Chadwick M., Allen C.S., Sime L.C., Crosta X. & Hillenbrand C.-D. 2022b. How does the Southern Ocean
323 palaeoenvironment during Marine Isotope Stage 5e compare to the modern? *Marine*
324 *Micropaleontology*, **170**: 102066.

325 Chadwick M., Allen C.S., Sime L.C. & Hillenbrand C.D. 2020. Analysing the timing of peak warming and
326 minimum winter sea-ice extent in the Southern Ocean during MIS 5e. *Quaternary Science Reviews*,
327 **229**: 106134.

328 Dotto T.S., Naveira Garabato A., Bacon S., Tsamados M., Holland P.R., Hooley J., Frajka-Williams E.,
329 Ridout A. & Meredith M.P. 2018. Variability of the Ross Gyre, Southern Ocean: Drivers and Responses
330 Revealed by Satellite Altimetry. *Geophysical Research Letters*, **45**: 6195-6204.

331 Dyer B., Austermann J., D'Andrea W.J. & Raymo M.E. 2021. Sea-level trends across The Bahamas
332 constrain peak last interglacial ice melt. *PNAS*, **118** (33): e2026839118.

333 Dutton A., Carlson A.E., Long A.J., Milne G.A., Clark P.U., DeConto R., Horton B.P., Rahmstorf S. &
334 Raymo M.E. 2015. Sea-level rise due to polar ice-sheet mass loss during past warm periods. *Science*,
335 **349** (6244): aaa4019.

336 Fetterer F., Knowles K., Meier W.N., Savoie M. & Windnagel A.K. 2017. Sea Ice Index, Version 3.
337 *Boulder, Colorado USA*. NSIDC: National Snow and Ice Data Center.

338 Fischer H., Meissner K.J., Mix A.C., Abram N.J., Austermann J., Brovkin V., Capron E., Colombaroli D.,
339 Daniau A.-L., Dyez K.A., Felis T., Finkelstein S.A., Jaccard S.L., McClymont E.L., Rovere A., Sutter J., Wolff

340   E.W., Affolter S., Bakker P., Ballesteros-Cánovas J.A., Barbante C., Caley T., Carlson A.E., Churakova O.,
341   Cortese G., Cumming B.F., Davis B.A.S., de Vernal A., Emile-Geay J., Fritz S.C. et al. 2018. Palaeoclimate
342   constraints on the impact of 2 °C anthropogenic warming and beyond. *Nature Geoscience*, **11** (7): 474-
343   485.

344   Ghadi P., Nair A., Crosta X., Mohan R., Manoj M.C. & Meloth T. 2020. Antarctic sea-ice and
345   palaeoproductivity variation over the last 156,000 years in the Indian sector of Southern Ocean.
346   *Marine Micropaleontology*, **160**: 101894.

347   Guarino M.-V., Sime L.C., Schröeder D., Malmierca-Vallet I., Rosenblum E., Ringer M., Ridley J., Feltham
348   D., Bitz C., Steig E.J., Wolff E., Stroeve J. & Sellar A. 2020. Sea-ice-free Arctic during the Last Interglacial
349   supports fast future loss. *Nature Climate Change*, **10** (10): 928-932.

350   Guarino M.V., Sime L.C., Schroeder D. & Ridley J. 2022, *in review*. The first 250 years of the Heinrich
351   11 iceberg discharge: Last Interglacial HadGEM3-GC3.1 simulations for CMIP6-PMIP4. *Climate of the
352   Past Discussions [preprint]*. (https://cp.copernicus.org/preprints/cp-2021-187/).

353   Hall A. 2004. The Role of Surface Albedo Feedback in Climate. *Journal of Climate*, **17**: 1550-1568.

354   Hobbs W.R., Massom R., Stammerjohn S., Reid P., Williams G. & Meier W. 2016. A review of recent
355   changes in Southern Ocean sea ice, their drivers and forcings. *Global and Planetary Change*, **143**: 228-
356   250.

357   Holloway M.D., Sime L.C., Allen C.S., Hillenbrand C.-D., Bunch P., Wolff E. & Valdes P.J. 2017. The
358   spatial structure of the 128 ka Antarctic sea ice minimum. *Geophysical Research Letters*, **44** (21):
359   11129-11139.

360   Holloway M.D., Sime L.C., Singarayer J.S., Tindall J.C. & Valdes P.J. 2018. Simulating the 128-ka
361   Antarctic Climate Response to Northern Hemisphere Ice Sheet Melting Using the Isotope-Enabled
362   HadCM3. *Geophysical Research Letters*, **45** (21): 11921-11929.

363   Madec G., Bourdalle-Badie R., Chanut J., Clementi E., Coward A., Ethe C., Iovino D., Lea D., Levy C.,
364   Lovato T., Martin N., Masson S., Mocavero S., Rousset C., Storkey D., Vancoppenolle M., Mueller S.,
365   Nurser G., Bell M. & Samson G. 2019. *NEMO ocean engine*: Notes Du Pole De Modelisation De L'institut
366   Pierre-simon Laplace (IPSL).

367   Maksym T. 2019. Arctic and Antarctic Sea Ice Change: Contrasts, Commonalities, and Causes. *Ann Rev
368   Mar Sci*, **11**: 187-213.

369   Marino G., Rohling E.J., Rodriguez-Sanz L., Grant K.M., Heslop D., Roberts A.P., Stanford J.D. & Yu J.
370   2015. Bipolar seesaw control on last interglacial sea level. *Nature*, **522** (7555): 197-201.

371   Menary M.B., Kuhlbrodt T., Ridley J., Andrews M.B., Dimdore-Miles O.B., Deshayes J., Eade R., Gray L.,
372   Ineson S., Mignot J., Roberts C.D., Robson J., Wood R.A. & Xavier P. 2018. Preindustrial Control
373   Simulations With HadGEM3-GC3.1 for CMIP6. *Journal of Advances in Modeling Earth Systems*, **10**:
374   3049-3075.

375   Meredith M., Sommerkorn M., Cassotta S., Derksen C., Ekaykin A., Hollowed A., Kofinas G., Mackintosh
376   A., Melbourne-Thomas J., Muelbert M.M.C., Ottersen G., Pritchard H. & Schuur E.A.G. 2019. Polar
377   Regions. In: *IPCC Special Report on the Ocean and Cryosphere in a Changing Climate*, Portner H.O.,
378   Roberts D.C., Masson-Delmotte V. et al. Eds. Cambridge University Press**:** 203-320.

379   Merino N., Jourdain N.C., Le Sommer J., Goosse H., Mathiot P. & Durand G. 2018. Impact of increasing
380   antarctic glacial freshwater release on regional sea-ice cover in the Southern Ocean. *Ocean Modelling*,
381   **121**: 76-89.

382 Nghiem S.V., Rigor I.G., Clemente-Colón P., Neumann G. & Li P.P. 2016. Geophysical constraints on the
383 Antarctic sea ice cover. *Remote Sensing of Environment*, **181**: 281-292.

384 Otto-Bliesner B.L., Braconnot P., Harrison S.P., Lunt D.J., Abe-Ouchi A., Albani S., Bartlein P.J., Capron
385 E., Carlson A.E., Dutton A., Fischer H., Goelzer H., Govin A., Haywood A., Joos F., LeGrande A.N.,
386 Lipscomb W.H., Lohmann G., Mahowald N., Nehrbass-Ahles C., Pausata F.S.R., Peterschmitt J.-Y.,
387 Phipps S.J., Renssen H. & Zhang Q. 2017. The PMIP4 contribution to CMIP6 – Part 2: Two interglacials,
388 scientific objective and experimental design for Holocene and Last Interglacial simulations.
389 *Geoscientific Model Development*, **10** (11): 3979-4003.

390 Otto-Bliesner B.L., Brady E.C., Zhao A., Brierley C., Axford Y., Capron E., Govin A., Hoffman J., Isaacs E.,
391 Kageyama M., Scussolini P., Tzedakis P.C., Williams C., Wolff E., Abe-Ouchi A., Braconnot P., Ramos
392 Buarque S., Cao J., de Vernal A., Guarino M.V., Guo C., LeGrande A.N., Lohmann G., Meissner K.,
393 Menviel L., Nisancioglu K., O'Ishi R., Salas Y Melia D., Shi X., Sicard M. et al. 2021. Large-scale features
394 of Last Interglacial climate: results from evaluating the *lig127k* simulations for the Coupled Model
395 Intercomparison Project (CMIP6)-Paleoclimate Modeling Intercomparison Project (PMIP4). *Climate of
396 the Past*, **17**: 63-94.

397 Purich A., England M.H., Cai W., Chikamoto Y., Timmermann A., Fyfe J.C., Frankcombe L., Meehl G.A.
398 & Arblaster J.M. 2016. Tropical Pacific SST Drivers of Recent Antarctic Sea Ice Trends. *Journal of
399 Climate*, **29** (24): 8931-8948.

400 Rayner N.A., Parker D.E., Horton E.B., Folland C.K., Alexander L.V., Rowell D.P., Kent E.C. & Kaplan A.
401 2003. Global analyses of sea surface temperature, sea ice, and night marine air temperature since the
402 late nineteenth century. *Journal of Geophysical Research*, **108** (D14): 4407.

403 Ridley J., Menary M.B., Kuhlbrodt T., Andrews M.B. & Andrews T. 2018a. MOHC HadGEM3-GC31-LL
404 model output prepared for CMIP6 CMIP. *Earth System Grid Federation*.

405 Ridley J.K., Blockley E.W., Keen A.B., Rae J.G.L., West A.E. & Schroeder D. 2018b. The sea ice model
406 component of HadGEM3-GC3.1. *Geoscientific Model Development*, **11** (2): 713-723.

407 Rintoul S.R. 2018. The global influence of localized dynamics in the Southern Ocean. *Nature*, **558**
408 (7709): 209-218.

409 Rosenblum E. & Eisenman I. 2017. Sea Ice Trends in Climate Models Only Accurate in Runs with Biased
410 Global Warming. *Journal of Climate*, **30** (16): 6265-6278.

411 Sime L.C., Wolff E.W., Oliver K.I. & Tindall J.C. 2009. Evidence for warmer interglacials in East Antarctic
412 ice cores. *Nature*, **462** (7271): 342-345.

413 Stone E.J., Capron E., Lunt D.J., Payne A.J., Singarayer J.S., Valdes P.J. & Wolff E.W. 2016. Impact of
414 meltwater on high-latitude early Last Interglacial climate. *Climate of the Past*, **12** (9): 1919-1932.

415 Vernet M., Geibert W., Hoppema M., Brown P.J., Haas C., Hellmer H.H., Jokat W., Jullion L., Mazloff
416 M., Bakker D.C.E., Brearley J.A., Croot P., Hattermann T., Hauck J., Hillenbrand C.D., Hoppe C.J.M.,
417 Huhn O., Koch B.P., Lechtenfeld O.J., Meredith M.P., Naveira Garabato A.C., Nöthig E.M., Peeken I.,
418 Rutgers van der Loeff M.M., Schmidtko S., Schröder M., Strass V.H., Torres-Valdés S. & Verdy A. 2019.
419 The Weddell Gyre, Southern Ocean: Present Knowledge and Future Challenges. *Reviews of
420 Geophysics*, **57** (3): 623-708.

421 Walters D., Boutle I., Brooks M., Melvin T., Stratton R., Vosper S., Wells H., Williams K., Wood N., Allen
422 T., Bushell A., Copsey D., Earnshaw P., Edwards J., Gross M., Hardiman S., Harris C., Heming J.,
423 Klingaman N., Levine R., Manners J., Martin G., Milton S., Mittermaier M., Morcrette C., Riddick T.,
424 Roberts M., Sanchez C., Selwood P., Stirling A. et al. 2017. The Met Office Unified Model Global

425 Atmosphere 6.0/6.1 and JULES Global Land 6.0/6.1 configurations. *Geoscientific Model Development*,
426 **10** (4): 1487-1520.

427 Wang Z. 2013. On the response of Southern Hemisphere subpolar gyres to climate change in coupled
428 climate models. *Journal of Geophysical Research: Oceans*, **118** (3): 1070-1086.

429 Wilson D.J., Bertram R.A., Needham E.F., van de Flierdt T., Welsh K.J., McKay R.M., Mazumder A.,
430 Riesselman C.R., Jimenez-Espejo F.J. & Escutia C. 2018. Ice loss from the East Antarctic Ice Sheet during
431 late Pleistocene interglacials. *Nature*, **561** (7723): 383-386.